

Technical Report

Title: *Assessment of Porosity Data and Gas Phase Presence in DGR Cores*

Document ID: TR-08-34


Authors: Sean Sterling, Richard Jackson, Robert Walsh, Dru Heagle, and Ian Clark (University of Ottawa)

Revision: 0

Date: April 15, 2011

DGR Site Characterization Document
Geofirma Engineering Project 08-200



Geofirma Engineering DGR Site Characterization Document		
Title:	Assessment of Porosity Data and Gas Phase Presence in DGR Cores	
Document ID:	TR-08-34	
Revision Number:	0	Date: April 15, 2011
Authors:	Sean Sterling, Richard Jackson, Robert Walsh, Dru Heagle and Ian Clark, (University of Ottawa)	
Technical Review:	Kenneth Raven; Mark Jensen, Laura Kennell, Andy Parmenter (NWMO)	
QA Review:	John Avis	
Approved by:	 Kenneth Raven	

Document Revision History		
Revision	Effective Date	Description of Changes
0	April 15, 2011	Initial release

TABLE OF CONTENTS

1	INTRODUCTION	1
2	DATA SOURCES	1
3	PETROPHYSICAL DATA.....	2
3.1	Liquid and Total Porosity.....	2
3.1.1	Definitions and Experimental Methods	2
3.1.2	Converting Water-Loss Porosity to Liquid Porosity.....	4
3.1.3	Porosity Values.....	7
3.1.4	Assessment of Porosity Data.....	11
3.2	Fluid Saturations	14
3.2.1	Definitions and Experimental Methods	14
3.2.2	Fluid Saturation Values.....	15
3.2.3	Assessment of Fluid Saturation Data.....	22
4	GEOCHEMICAL DATA	26
4.1	Geochemical Partitioning of Gas - Experimental Methods	26
4.2	Methane and Carbon Dioxide Solubility Data.....	26
4.2.1	Methane Solubility	27
4.2.2	Carbon Dioxide Solubility.....	28
5	GEOMECHANICAL DATA	31
5.1	Microcrack Relaxation Porosity – Analytical Methods	31
5.2	Microcrack Relaxation Porosity Data.....	33
6	CONCLUSIONS	36
7	REFERENCES	37

LIST OF TABLES

Table 1	Summary of Porosity Measurements for DGR Core Samples.....	3
Table 2	Formational Average Pore Fluid Properties	5
Table 3	Summary of Total, Liquid and Water-Loss Porosity (%) by Formation/Unit/Member	10
Table 4	Summary of Total, Liquid and Water-Loss Porosity (%) by Formation Grouping	11
Table 5	Dean Stark Fluid Saturations for DGR-2 Core Samples	16
Table 6	Dean Stark Fluid Saturations for DGR-3 Core Samples	17
Table 7	Dean Stark Fluid Saturations for DGR-4 Core Samples	18
Table 8	Dean Stark Fluid Saturations for DGR-5 Core Samples	18
Table 9	Dean Stark Fluid Saturations for DGR-6 Core Samples	19
Table 10	NMR and Dean Stark Fluid Saturations for DGR-4, DGR-5 and DGR-6 Core Samples (%)	24
Table 11	Summary of Fluid Saturation Values by Formation Grouping.....	25

LIST OF FIGURES

Figure 1	Liquid Density and TDS Concentration Profiles for US-8 and DGR Boreholes	6
Figure 2	Depth Profile of Total Porosity Measurements from DGR Cores.....	8
Figure 3	Depth Profile of Liquid Porosity Measurements from DGR Cores	9
Figure 4	Comparison of Total and Liquid Porosity Measured by Core Labs and UniBern on the Same DGR Core Plugs.....	12
Figure 5	Comparison of Total and Liquid Porosity Measured by Core Labs on the Same DGR Core Plugs	13
Figure 6	Comparison of ratio of unconfined to confined total porosity versus confined total porosity measured by Core Labs on DGR-3 and DGR-4 core plugs. Arithmetic mean ratios for major groups of formations are also shown.	14
Figure 7	Profile of Water and Gas Saturations in DGR Cores	19
Figure 8	Profile of Oil Saturations in DGR Cores	20
Figure 9	Water Saturations (S_w) for DGR-2, DGR-3, DGR-4, DGR-5 and DGR-6 Cores Plotted Against Their Total Porosity	21
Figure 10	Gas Saturations (S_g) for DGR-2, DGR-3, DGR-4, DGR-5 and DGR-6 Cores Plotted Against Their Total Porosity	22
Figure 11	Fractional Uncertainty in the Water Saturation vs. Total Porosity in DGR Cores	23
Figure 12	Comparison of Methods of Measuring Fluid Saturations in DGR-4 cores	25
Figure 13	Cross Plot of Apparent CH_4 and $Na+Cl$ Porewater Concentrations Compared to Calculated CH_4 Solubility in DGR-3.....	27
Figure 14	Cross Plot of Apparent CH_4 and $Na+Cl$ Porewater Concentrations Compared to Calculated CH_4 Solubility in DGR-4.....	28
Figure 15	Cross Plot of Apparent CO_2 and $Na+Cl$ Porewater Concentrations Compared to Calculated CO_2 Solubility in DGR-3.	29
Figure 16	Cross Plot of Apparent CO_2 and $Na+Cl$ Porewater Concentrations Compared to Calculated CO_2 Solubility in DGR-4.	30
Figure 17	Gas-Oil Ratio (R_G) as a Function of In-Situ Fluid Pressure for Gases Composed of Different Amounts of Methane and Carbon Dioxide	31
Figure 18	Determination of relaxation porosity from volumetric strain data – above Georgian Bay Formation shale (491.32 mBGS) and below Cobourg Formation limestone (675.06 mBGS) in DGR-3.	34
Figure 19	Profile Comparison of Gas-Phase Porosity (i.e., $S_g \times$ total porosity) and Microcrack Relaxation Porosity in DGR Cores.	35

LIST OF APPENDICES

APPENDIX A	Volumetric Strain Curves – DGR-2, DGR-3 and DGR-4 Cores
------------	---

1 Introduction

Geofirma Engineering Ltd. (formerly Intera Engineering Ltd.) has been contracted by the Nuclear Waste Management Organization (NWMO), on behalf of Ontario Power Generation, to implement the Geoscientific Site Characterization Plan (GSCP) for the Bruce nuclear site located near Tiverton, Ontario. The purpose of this site characterization work is to assess the suitability of the geological formations beneath the Bruce nuclear site to host a Deep Geologic Repository (DGR) to store low-level and intermediate-level radioactive waste.

The GSCP consists of three phases of borehole drilling and investigations. The Phase 1 GSCP is described by Intera Engineering Ltd. (2006) and included the drilling and testing of two deep boreholes, DGR-1 and DGR-2 to total depths of 462.9 and 862.3 metres below ground surface (mBGS), respectively. Phase 1 drilling and testing was completed between December 2006 and December 2007. The Phase 2 GSCP is described by Intera Engineering Ltd. (2008a). Phase 2 is divided into two sub-phases, 2A and 2B. Phase 2A included the drilling of two vertical boreholes, DGR-3 and DGR-4, which were drilled into the top of the Cambrian sandstone at depths of approximately 869 and 857 mBGS, respectively. Phase 2A was completed between March 2008 and September 2009. Phase 2B consisted of drilling of two inclined boreholes, DGR-5 and DGR-6, which were drilled into the Kirkfield and Gull River Formations at depths of approximately 807 and 903 metres length below ground surface (mLBGS), respectively. Phase 2B was completed between December 2008 and June 2010.

As part of the GSCP, Geofirma Engineering Ltd. contracted with various laboratories to complete petrophysical (Core Laboratories), geochemical (University of Ottawa, University of New Brunswick, University of Bern) and geomechanical (CANMET) testing on samples of core collected from boreholes DGR-1, DGR-2, DGR-3, DGR-4, DGR-5 and DGR-6. This Technical Report describes the testing and data analysis undertaken by Intera to investigate the possible presence of a gas phase in portions of the pore volume, in addition to dissolved gas contained within the brine, as well as any oil measured in the DGR cores. One dataset that supports the presence of a gas phase in the Paleozoic bedrock below the Bruce nuclear site is porosity – more specifically, the comparison of total (physical) porosity (ϕ_T) and liquid porosity (ϕ_W). Therefore, as part of the gas-phase assessment, a methodology is presented that allows for the comparison of liquid porosity data between different laboratories. Such a methodology is necessary because the different laboratories used differing calculation techniques and assumptions of porewater composition.

Work described in this Technical Report was completed following the general requirements of the DGR Project Quality Plan (Intera Engineering Ltd., 2009a).

2 Data Sources

The work associated with the collection of the data presented in this Technical Report was completed in accordance with various test plans, most of which have been reported previously in other Technical Reports. Individual laboratory methods described, and sample measurements reported to date, are included in the following Technical Reports:

Residual Fluid Saturation Data

- TR-07-18 – Lab Petrophysical Testing of DGR-2 Core (Intera Engineering Ltd., 2010a);
- TR-08-28 – Lab Petrophysical Testing of DGR-3 and DGR-4 Core (Intera Engineering Ltd., 2010b); and,
- TR-09-08 – Lab Petrophysical Testing of DGR-5 and DGR-6 Core (Geofirma Engineering Ltd., 2011a).

Total and Liquid Porosity Data

- TR-07-18 – Lab Petrophysical Testing of DGR-2 Core (Intera Engineering Ltd., 2010a);
- TR-07-21 – Porewater and Gas Analyses of DGR-1 and DGR-2 Core (Intera Engineering Ltd., 2010c);
- TR-07-17 – Lab Diffusion Testing of DGR-2 Core (Intera Engineering Ltd., 2010d);

- TR-08-06 – Porewater Characterization – DGR-2 (Koroleva et al., 2009);
- TR-08-28 – Lab Petrophysical Testing of DGR-3 and DGR-4 Core (Intera Engineering Ltd., 2010b);
- TR-08-19 – Porewater and Gas Analyses in DGR-3 and DGR-4 Core (Intera Engineering Ltd., 2010e);
- TR-08-27 – Lab Diffusion Testing of DGR-3 and DGR-4 Core (Intera Engineering Ltd., 2010f);
- TR-08-40 – Porewater Characterization – DGR-3 and DGR-4 (Hobbs et al, 2011);
- TR-09-04 – Porewater Analyses in DGR-5 and DGR-6 Core (Geofirma Engineering Ltd., 2011b); and
- TR-09-08 – Lab Petrophysical Testing of DGR-5 and DGR-6 Core (Geofirma Engineering Ltd., 2011a).

Data Used to Correct for Brine Density

- TR-07-11 – Opportunistic Groundwater Sampling in DGR-1 and DGR-2 (Intera Engineering Ltd., 2010g);
- TR-07-17 – Lab Diffusion Testing of DGR-2 Core (Intera Engineering Ltd., 2010d);
- TR-07-21 – Porewater and Gas Analyses in DGR-1 and DGR-2 Core (Intera Engineering Ltd., 2010c);
- TR-08-08 – Initial Groundwater Monitoring, US-3, US-7, US-8 (Intera Engineering Ltd., 2010h);
- TR-08-18 – Opportunistic Groundwater Sampling in DGR-3 and DGR-4 (Intera Engineering Ltd., 2010i);
- TR-08-19 – Porewater and Gas Analyses in DGR-3 and DGR-4 Core (Intera Engineering Ltd., 2010e);
- TR-08-27 – Lab Diffusion Testing of DGR-3 and DGR-4 Core (Intera Engineering Ltd., 2010f); and,
- TR-09-04 – Porewater Analyses in DGR-5 and DGR-6 Core (Geofirma Engineering Ltd., 2011b).

Geochemical Partitioning of Gas

- TR-07-21 - Porewater and Gas Analyses in DGR-1 and DGR-2 Core (Intera Engineering Ltd., 2010c);
- TR-08-19 – Porewater and Gas Analyses in DGR-3 and DGR-4 Core (Intera Engineering Ltd., 2010f); and,
- TR-09-04 – Porewater Analyses in DGR-5 and DGR-6 Core (Geofirma Engineering Ltd., 2010h).

Geomechanical – Microcrack Relaxation Porosity Data

- TR-07-03 – Laboratory Geomechanical Strength Testing of DGR-1 and DGR-2 Core (Intera Engineering Ltd., 2009b);
- TR-08-24 – Laboratory Geomechanical Strength Testing of DGR-3 and DGR-4 Core (Intera Engineering Ltd., 2010j); and
- TR-09-07 – Laboratory Geomechanical Strength Testing of DGR-2 to DGR-6 Core (Geofirma Engineering Ltd., 2011c).

3 Petrophysical Data

3.1 Liquid and Total Porosity

3.1.1 Definitions and Experimental Methods

Porosity is a general term used to describe the fraction of the volume of voids over the total rock volume. Three types of porosity are defined in this Technical Report to differentiate the type of fluid occupying the void space and the measurements made by different testing laboratories: total porosity, liquid porosity and water-loss porosity. Total porosity is the sample volume not occupied by mineral grains (i.e., total volume of voids) divided by the volume of the sample, and comprises the cumulative total volume of water, oil and gas filled pore spaces. For samples without any significant or measureable oil phase the total porosity can be approximated as the sum of water-filled and gas-filled pore space. Liquid porosity is the volume of the voids occupied by liquid (i.e., pure water plus dissolved solutes and liquid petroleum such as oil and gas) divided by the total volume of the sample. Water-loss porosity is the volume of the voids occupied by pure water divided by the total volume of the sample. Total porosity should equal liquid porosity plus porosity occupied by any gas phase (e.g., methane).

Total porosity and/or water-loss porosity were measured on DGR rock cores by Core Laboratories (Core Labs), University of Ottawa (UofO), University of New Brunswick (UNB) and University of Bern (UniBern) as part of petrophysical, diffusion and porewater testing programs. Several of these laboratories also reported liquid porosities by correcting the water-loss porosities for an assumed brine density, which was individually selected by each lab. As different assumptions for brine density do not allow a direct comparison between lab data, all porosity data was corrected by Intera using a consistent approach as described in Section 3.1.2.

Table 1 summarizes the various approaches taken by individual laboratories to determine DGR core porosity, as well as additional calculations undertaken in this report to provide a common basis for comparison of different porosity data.

Table 1 Summary of Porosity Measurements for DGR Core Samples

<i>Test Element</i>	<i>UniBern</i>	<i>UofO</i>	<i>UNB</i>	<i>Core Labs</i>
Reported measurements	98 total porosity 21 liquid porosity 71 water-loss porosity	232 water content	72 liquid porosity	83 total porosity and water saturation
Methods	Bulk dry/grain density calculation using Archimedes Principle (paraffin displacement)	Bulk dry/grain density calculation using Vacuum Distillation	Bulk dry/grain density calculation using Archimedes Principle (brine displacement)	Boyles Law gas expansion, Dean Stark fluid saturations
Sample size	~4-5 g plug (total)	~30 g crushed	~40-100 g disc	~150 g plug
	~60-420 g (water-loss)			
Drying temperature	40°C and 105°C	150°C	105°C	105°C
Drying time (days) range and (average)	48-135 (99) @ 40°C 12-174 (92) @ 105°C	6 hrs vacuum distillation	7 to 89 (21)	2 to 7 vacuum oven
Correction for brine density	1.3 g/cm ³ (< 830 mBGS) 1.2 g/cm ³ (> 830 mBGS)	not corrected	variable	1.187 g/cc (TDS=250 g/kg)
Additional Intera calculations	Reduced to water-loss porosity and then converted to liquid porosity based on formation average TDS	Converted water content to water-loss porosity and then to liquid porosity based on formation average TDS	Reduced to water-loss porosity and then converted to liquid porosity based on formation average TDS	Calculated water-loss porosity from S _w and then converted to liquid porosity based on formation average TDS

A total of 485 core samples were analysed for physical and/or liquid porosity by four laboratories, as summarized in Table 1, including:

- *University of Bern* – 71 samples analysed for both total porosity and liquid (DGR-2) or water-loss (DGR-3 and DGR-4) porosity, plus an additional 27 samples analysed for total porosity only (DGR-2). Each porosity measurement was completed on different sub-samples taken from the same preserved core sample, as described in Koroleva et al. (2009). Total porosity sub-samples were 4-5 g plugs and liquid porosity sub-samples were 60-420 g segments (edges chipped off sample). Liquid porosity values were reported

assuming brine density at halite saturation (1.3 g/cc above 830 mBGS and 1.2 g/cc below 830 mBGS) and determined using gravimetric techniques by drying at 105°C. All UniBern liquid porosity data were reduced to water-loss porosity values for comparison to similar data from other labs;

- *University of Ottawa* – 232 samples analysed for water content (not corrected for density) as described in TR-07-21 (Clark et al. 2010), TR-08-19 and TR-09-04. Analysis completed on ~30 g sub samples of crushed core (2-3 mm diameter pieces) and dried using vacuum distillation techniques at 150°C. All University of Ottawa volumetric water content values were converted to water-loss porosity values for comparison to similar data from other labs;
- *University of New Brunswick* – 72 samples analysed for liquid porosity using 40-100 g discs of core, each 1 cm thick, as described in TR-07-17 and TR-08-27. Liquid porosity values reported are based on assumption of various brine densities based on geological formation grouping and determined using gravimetric techniques by oven drying at 105°C. All University of New Brunswick liquid porosity data were reduced to water-loss porosity values for comparison to similar data from other labs.
- *Core Laboratories* – 83 samples analysed for total porosity and water saturation on the same ~150 g core plug (horizontal and vertical). Total porosity measured by Boyle's gas law expansion (He) on "clean and dried" samples under a confining stress of 17 kPa/m (DGR-2) and 34 kPa/m (DGR-3 and DGR-4) to replicate the depth-specific hydrostatic in-situ stress (DGR-5 and DGR-6 samples analysed with no confining stress). Water-loss porosity values were calculated using lab data from Dean Stark fluid saturation measurements. For DGR-3 and DGR-4 cores, Core Labs also measured total porosity on unconfined cores, such that a direct estimate of the magnitude of porosity increase due to core relaxation could be determined. For DGR-5 and DGR-6 cores, Core Labs measured total porosity and liquid porosity using Dean Stark methods and using Nuclear Magnetic Resonance (NMR)/He gas expansion methods on the same cores. The DGR-5 and DGR-6 tests were done on unconfined cores, as core confinement was not possible during NMR testing.

3.1.2 Converting Water-Loss Porosity to Liquid Porosity

In order to compare liquid porosity measurements between the different laboratories, a consistent density correction needs to be applied. Therefore, all lab data was reduced to water-loss porosity values and was converted to liquid porosity values by assuming a mass of salts for each sample based on average brine (liquid) densities and total dissolved solids (TDS) concentrations for each formation. Table 2 and Figure 1 summarize the formational average values for liquid density, TDS and mass fraction of salts.

These formational average values were estimated using porewater chemistry data from the University of Ottawa (TR-07-21, TR-08-19, and TR-09-04), the University of New Brunswick (TR-07-17, TR-08-27), and groundwater chemistry data from opportunistic groundwater sampling (TR-07-11 and TR-08-18) and US-series borehole sampling (TR-08-08).

Table 2 Formational Average Pore Fluid Properties

Formation	Liquid Density (kg/m³)	Total Dissolved Solids, TDS (g/kg water)	Mass Fraction Salts, x (fraction)
Lucas	990	0.5	0.0005
Amherstburg	990	0.5	0.0005
Bois Blanc	993	0.5	0.0005
Bass Islands	993	3	0.003
Salina G	1001	6	0.006
Salina F	1004	15	0.015
Salina E	1029	63	0.059
Salina D	1043	143	0.125
Salina C	1093	211	0.172
Salina B	1143	279	0.218
B-Evaporite	1173	415	0.293
SalinaA2	1118	271	0.203
A2-Evaporite	1064	128	0.113
Salina A1 Upper	1020	47	0.045
Salina A1 Lower	1013	22	0.022
A1-Evaporite	1063	126	0.112
Salina A0	1180	1099	0.524
Guelph	1190	366	0.268
Goat Island	1234	320	0.242
Gasport	1165	338	0.253
Lions Head	1182	351	0.260
Fossil Hill	1181	350	0.259
Cabot Head	1197	376	0.273
Manitoulin	1179	349	0.259
Queenston	1210	405	0.288
Georgian Bay	1177	350	0.259
Blue Mountain	1179	345	0.257
Collingwood	1173	334	0.251
Cobourg	1128	249	0.200
Sherman Fall	1168	325	0.245
Kirkfield	1157	304	0.233
Coboconk	1132	256	0.204
Gull River	1148	287	0.223
Shadow Lake	1115	224	0.183
Cambrian	1113	221	0.181
Precambrian	1146	240	0.194

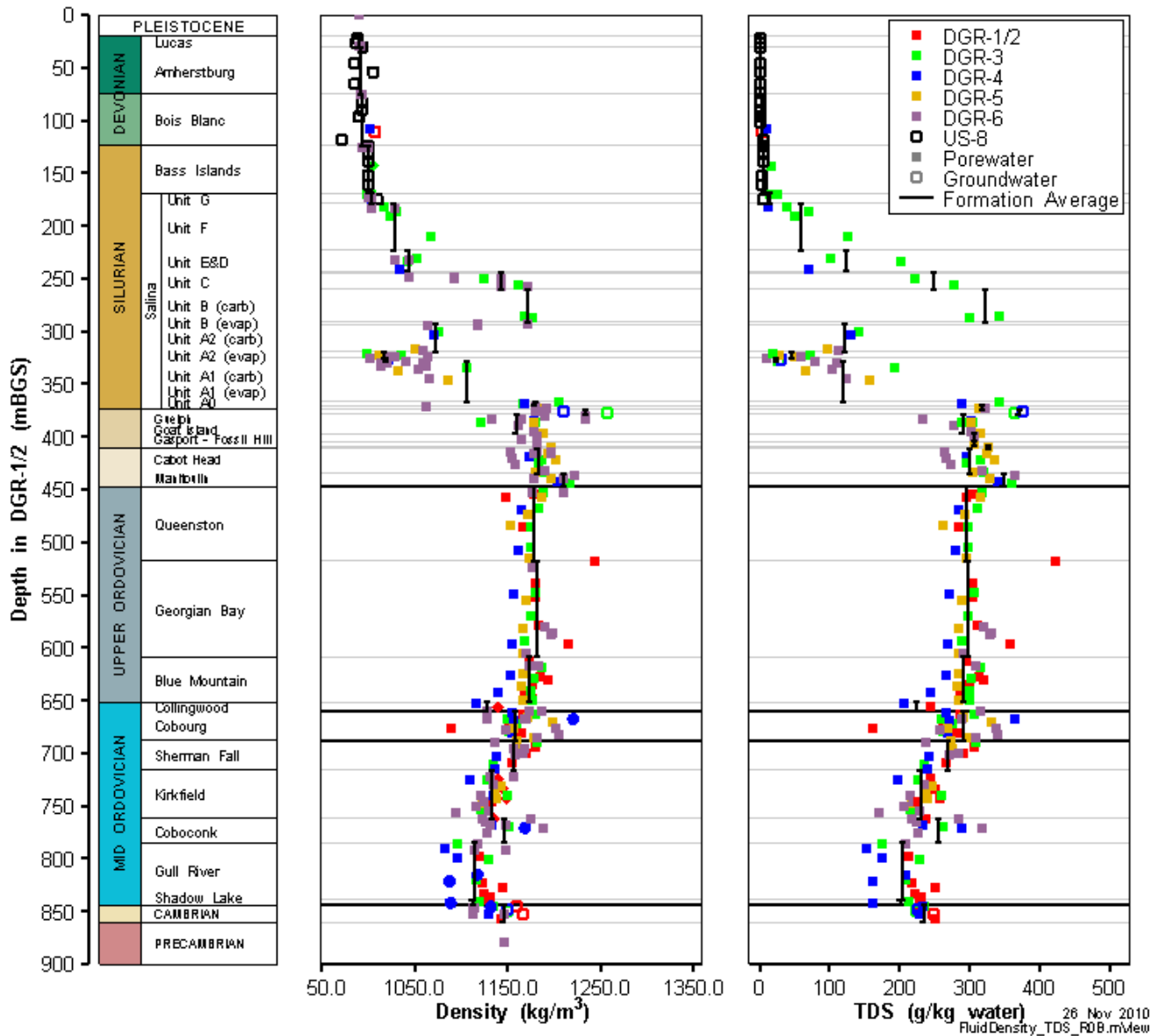


Figure 1 Liquid Density and TDS Concentration Profiles for US-8 and DGR Boreholes

To convert between water-loss porosity and liquid porosity, the following conversion was applied:

$$\phi_L = \phi_w \times \frac{V_b}{V_w} \quad [1]$$

where:

ϕ_L = liquid (i.e., brine) porosity = V_b/V_T ,

ϕ_w = water-loss porosity = V_w/V_T ,

V_b = volume of liquid (brine) = $M_b/\rho_b = (M_w + M_s) / \rho_b$,

M_b = mass of brine = mass of water + mass of salts = $M_w + M_s$,

ρ_b = formational average density of brine (Table 2),

V_w = volume of pure water = M_w/ρ_w ,

M_w = mass of pure water as determined from raw lab data, and

ρ_w = density of pure water, assumed to be 1000 kg/m³.

The mass fraction of salts (x) is defined as the mass of salts (M_s) divided by the mass of solution (i.e., brine, M_b) and is expressed as a fraction (i.e., percentage) between 0 and 1. For the purpose of these calculations, M_s is approximated as the concentration of total dissolved solids (TDS) expressed as a formational average value in units of grams of solute per kilogram pure water (g/kg water). Therefore, the mass fraction of water ($1-x$) can be defined as the mass of water (M_w) divided by the mass of brine (M_b), or:

x = formational average mass fraction of salts = $M_s/M_b = M_s / (M_w + M_s)$ as summarized in Table 2, and
 $(1-x)$ = formational average mass fraction of water = $M_w/M_b = M_w / (M_w + M_s)$.

By substitution of the above variables, the volumetric ratio of brine to pure water (V_b/V_w) can be expressed as:

$$\frac{V_b}{V_w} = \frac{(M_b \times \rho_w)}{(M_w \times \rho_b)} = \left(\frac{M_w + M_s}{M_w} \right) \times \left(\frac{\rho_w}{\rho_b} \right) = \frac{\rho_w}{\rho_b \times (1-x)} \quad [2]$$

and therefore Equation [1] becomes:

$$\phi_L = \phi_w \times \frac{V_b}{V_w} = \phi_w \times \left(\frac{\rho_w}{\rho_b \times (1-x)} \right) \quad [3]$$

3.1.3 Porosity Values

Figures 2 and 3 summarize the distribution of total and liquid porosity, respectively, for all 485 samples analysed and plotted against depth and bedrock formations. Figures 2 and 3 also show the calculated arithmetic mean porosity for each bedrock formation, member and unit. For the Ordovician shale formations two arithmetic mean values are plotted: one for “hard beds” as identified in the core logs and characterized by porosity values less than approximately 4%, and one for the remainder of the “shales”. DGR-3 and DGR-4 results are depth adjusted to appear at the relative position in the DGR-1/2 reference stratigraphy.

Table 3 summarizes the arithmetic mean values of the porosity data, and the number of samples used in each calculation, for each identified bedrock formation, member and unit. Table 4 summarizes the same data by groups of formations. Tables 3 and 4 also indicate the total number of samples where liquid porosity was calculated to be greater than total porosity from each bedrock formation, member or unit or formation group.

The highest measurements of both total and liquid porosity are within the Salina C Unit dolomitic shale, with a formational average of approximately 19.4 and 18.5%, respectively. The lowest formational average value of total porosity occurs in the Coboconk Formation (0.7%) and the lowest formational average value of liquid porosity occurs in the Fossil Hill Formation (0.5%).

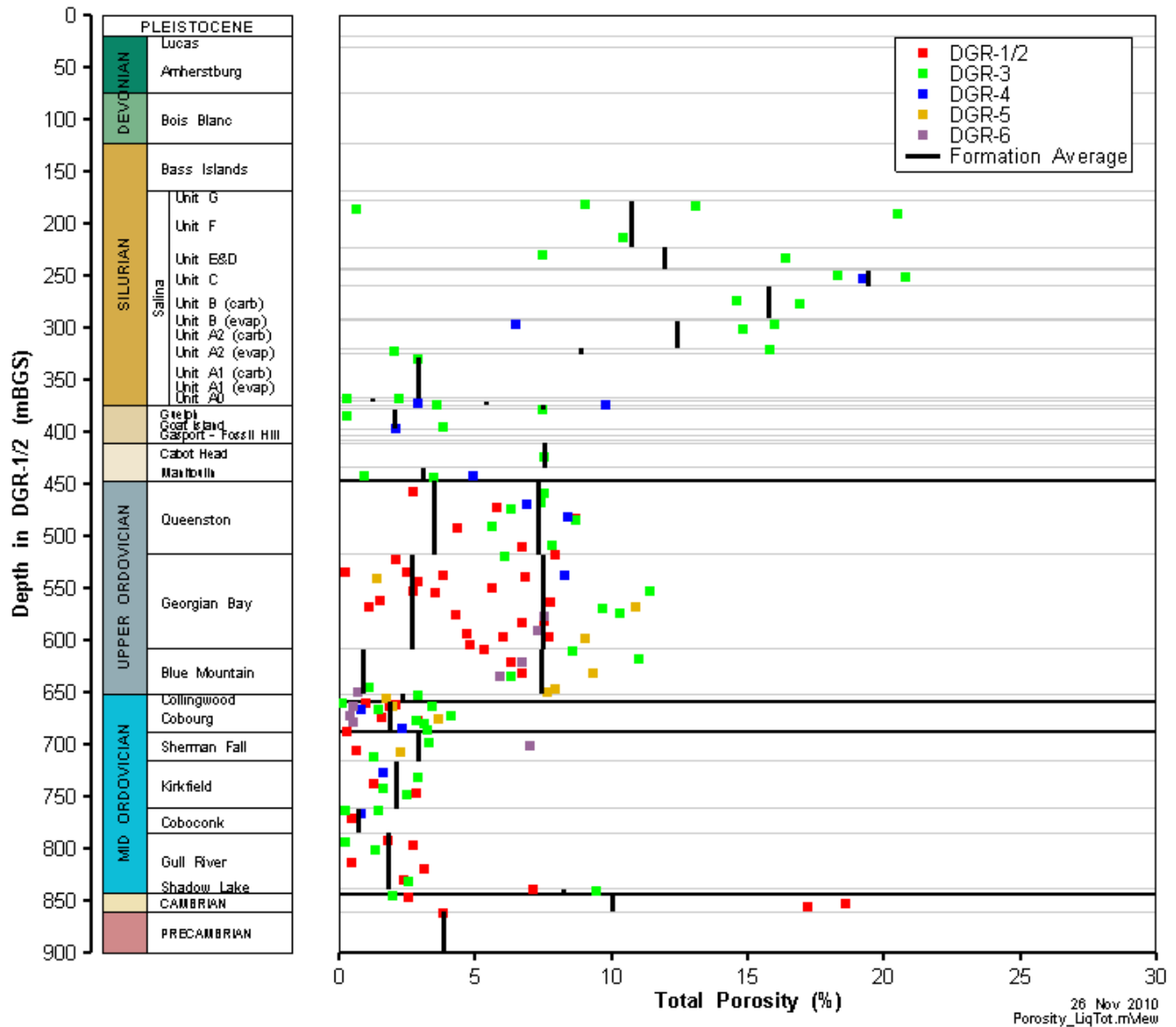


Figure 2 Depth Profile of Total Porosity Measurements from DGR Cores

The mean total porosity values for the Devonian and Silurian bedrock units show the greatest variation, ranging from 1.2% (Salina A1 Unit Evaporite) to 19.4% (Salina C Unit), with a formation grouping average of 8.9% (Table 3). This wide range of porosity values is due to the large variation of bedrock types including combinations of dolostones, shales, and evaporites. The mean total porosity for Ordovician shale formations ranges from 7.3 to 7.9%, with a formation grouping average of 7.4%, demonstrating consistency in the mean total porosity values for the relatively homogeneous shale units. Similarly, the mean total porosity values for Ordovician limestones and “hard beds” ranged from 0.7% (Coboconk) to 3.5% (Queenston – hard bed) with a formation grouping average of 1.9 to 2.5% (limestones and hard beds, respectively).

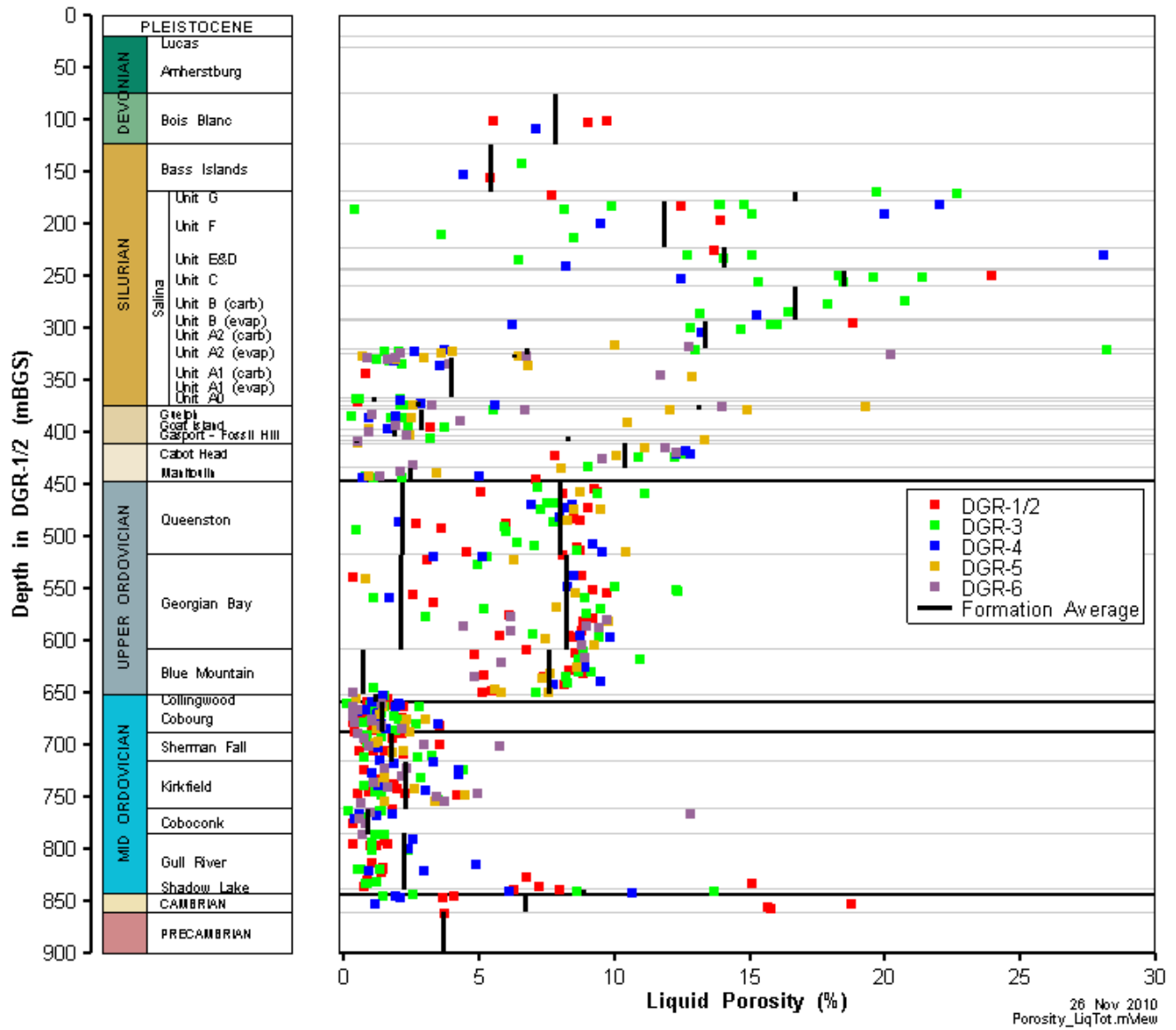


Figure 3 Depth Profile of Liquid Porosity Measurements from DGR Cores

Table 3 Summary of Total, Liquid and Water-Loss Porosity (%) by Formation/Unit/Member

<i>Formation, Member or Unit</i>	<i>(# Liq > Tot) / (# Tot & Liq)</i>	<i>Total Porosity</i>		<i>Liquid Porosity</i>		<i>Water-Loss Porosity</i>	
		<i>Mean</i>	<i>Count</i>	<i>Mean</i>	<i>Count</i>	<i>Mean</i>	<i>Count</i>
Lucas	NA	null	null	null	null	null	null
Amherstburg	NA	null	null	null	null	null	null
Bois Blanc	NA	null	0	7.8	4	7.8	4
Bass Islands	NA	null	0	5.5	3	5.4	3
Salina G Unit – shale	NA	null	0	16.7	3	16.5	3
Salina F Unit – shale	2/5 = 40%	10.7	5	11.9	14	11.5	14
Salina E Unit	1/2 = 50%	11.9	2	14.0	7	12.8	7
Salina D Unit	NA	null	null	null	null	null	null
Salina C Unit - shale	1/3 = 33%	19.4	3	18.5	7	16.5	7
Salina B Unit	2/2 = 100%	15.8	2	16.7	5	13.8	5
B Unit Evaporite	NA	null	null	null	null	null	null
Salina A2 Unit	3/3 = 100%	12.4	3	13.4	7	12.6	7
A2-Evaporite	0/2 = 0%	8.9	2	6.7	5	6.6	9
Salina A1 Unit Upper	NA	null	null	6.3	6	6.2	6
Salina A1 Unit Lower	0/1 = 0%	2.9	1	4.0	13	3.8	13
A1-Evaporite	1/2 = 50%	1.2	2	1.1	5	0.6	5
Salina A0 Unit	0/3 = 0%	5.4	3	2.7	7	2.4	7
Guelph	0/1 = 0%	7.5	1	13.1	5	12.3	5
Goat Island	0/3 = 0%	2.1	3	2.8	16	2.5	16
Gasport	NA	null	null	1.9	3	1.6	3
Lions Head	NA	null	null	8.3	2	7.2	2
Fossil Hill	NA	null	null	0.5	2	0.4	2
Cabot Head – shale	1/1 = 100%	7.5	1	10.4	15	9.1	15
Manitoulin	1/3 = 33%	3.1	3	2.4	10	2.1	10
Queenston - shale	8/14 = 57%	7.3	12	8.0	35	6.9	35
Queenston – hard beds	0/2 = 0%	3.5	2	2.2	4	1.9	4
Georgian Bay - shale	5/13 = 38%	7.5	18	8.2	39	7.2	39
Georgian Bay – hard beds	1/5 = 20%	2.7	11	2.1	9	1.9	9
Blue Mountain - shale	4/13 = 31%	7.4	11	7.6	30	6.7	30
Blue Mountain – hard beds	0/1 = 0%	0.9	2	0.7	2	0.6	2
Collingwood	0/3 = 0%	2.3	2	1.1	6	1.0	6
Cobourg	6/23 = 26%	1.9	20	1.4	59	1.3	59
Sherman Fall	1/7 = 14%	2.9	5	1.7	26	1.6	26
Kirkfield	1/6 = 18%	2.1	6	2.3	37	2.0	37
Coboconk	1/4 = 25%	0.7	4	0.9	14	0.8	14
Gull River	2/9 = 22%	1.8	8	2.2	31	2.0	31
Shadow Lake	1/2 = 50%	8.3	2	8.9	6	8.1	6
Cambrian	2/5 = 40%	10.1	4	6.7	10	6.2	10
Precambrian	0/1 = 0%	3.8	1	3.7	1	3.4	1

Table 4 Summary of Total, Liquid and Water-Loss Porosity (%) by Formation Grouping

<i>Formation Group</i>	<i>(# Liq > Tot) / (# Tot & Liq)</i>	<i>Total Porosity</i>		<i>Liquid Porosity</i>		<i>Water-Loss Porosity</i>	
		<i>Mean</i>	<i>Count</i>	<i>Mean</i>	<i>Count</i>	<i>Mean</i>	<i>Count</i>
Silurian and Devonian	12/31=39%	8.86	31	8.17	145	6.74	145
Ordovician shales	17/40=43%	7.41	41	7.96	104	1.67	104
Ordovician shale hard beds	1/9=11%	2.53	17	1.69	22	1.07	22
Ordovician limestones	11/52=22%	1.92	43	1.80	167	1.65	167
Shadow Lake and Cambrian sandstone	3/7=43%	9.46	6	7.52	16	5.79	16

Several factors contributing to the variability of porosity measurements have been identified by comparing the data and include: [1] small sample volume, [2] different measurement techniques with non-comparable laboratory measurement error, [3] low porosity resulting in low water yield and a higher percent error (as discussed in Section 3.1.3), and [4] general heterogeneity between nearby core samples.

3.1.4 Assessment of Porosity Data

As discussed in Section 3.1.1, total porosity is equal to the sum of liquid porosity and gas porosity, assuming there is no oil phase present in the pore spaces. Therefore, in order to assess whether a gas phase is present, liquid porosity values must be smaller compared to total porosity values for a particular sample. The only laboratories to measure both total and liquid porosity were Core Labs and UniBern; however UniBern completed the porosity measurements on different sub-sample specimens from the same preserved core sample.

Tables 3 and 4 summarize the number of core samples which had both total and liquid porosity values reported and further indicate the number of these core samples where liquid porosity was reported greater than total porosity, which by definition is not physically possible. Figure 4 shows the comparison of liquid and total porosity, colour coded by formation grouping, for all 139 samples where total and liquid porosity were measured on the same core sample. As shown, approximately 40% of the samples from the Devonian formations, Silurian formations and Upper Ordovician shales (i.e., samples with porosity greater than 4%) exhibit a liquid porosity greater than the corresponding total porosity for the same core sample. The number of samples from the Upper Ordovician “hard beds” and Middle Ordovician limestone units with liquid porosities greater than total porosities (i.e., samples with porosity less than 4%) is low at approximately 10 to 20%.

A possible reason for the inflated liquid porosity values in the Devonian/Silurian formations is the presence of gypsum ($\text{CaSO}_4 \cdot 2\text{H}_2\text{O}$) as a secondary mineral, which could release hydration water during sample heating and drying. Similarly, there is potential for the shales to release clay interlayer waters upon heating, particularly samples with higher smectite or montmorillonite content. These possible explanations for elevated liquid porosity values are supported by Lucia (1999) who identified “incomplete removal of all fluids during drying” and “alteration of rock fabrics that contain minerals with bound water such as gypsum and clay minerals” as two sources of inaccuracies in lab porosity measurements of carbonate rocks.

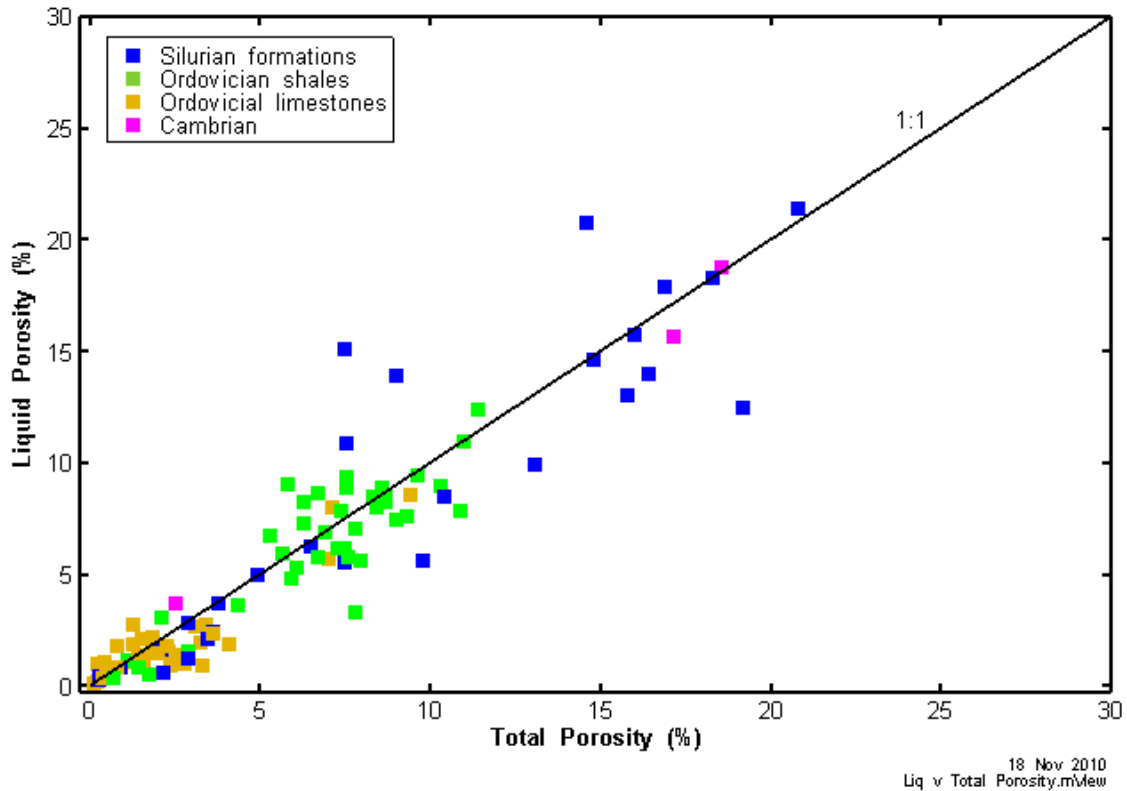


Figure 4 Comparison of Total and Liquid Porosity Measured by Core Labs and UniBern on the Same DGR Core Plugs

Another possible explanation for elevated liquid porosity measurements compared to total porosity is that some labs measure total and liquid porosity values using different methods and on different subsamples of core that are subject to different handling and sample preparation techniques. For example, UniBern performed total porosity measurements on a small core sample plug (4-5 g) and liquid porosity measurements on larger samples (60-420 g), which introduces error based on sample size and sample heterogeneity. The larger samples used for liquid porosity measurements may result in an averaged value that takes into account small heterogeneities that would not be measured in the individual smaller core plugs used for total porosity.

The increased error when comparing results from variable sample sizes is supported by comparing Figure 4, which compares the liquid vs. total porosity measurements completed on the same core samples by both UniBern (2 different sub samples) and Core Labs (both measurements on same core plug), to Figure 5, which presents a similar data comparison using only Core Labs data. In total, approximately 43% of UniBern samples were reported with liquid porosity greater than total porosity compared to 20% of Core Labs data. Therefore, the Core Labs data is considered to be the most reliable for comparing liquid vs. total porosity on the same sub-sample of core, however some inconsistencies remain.

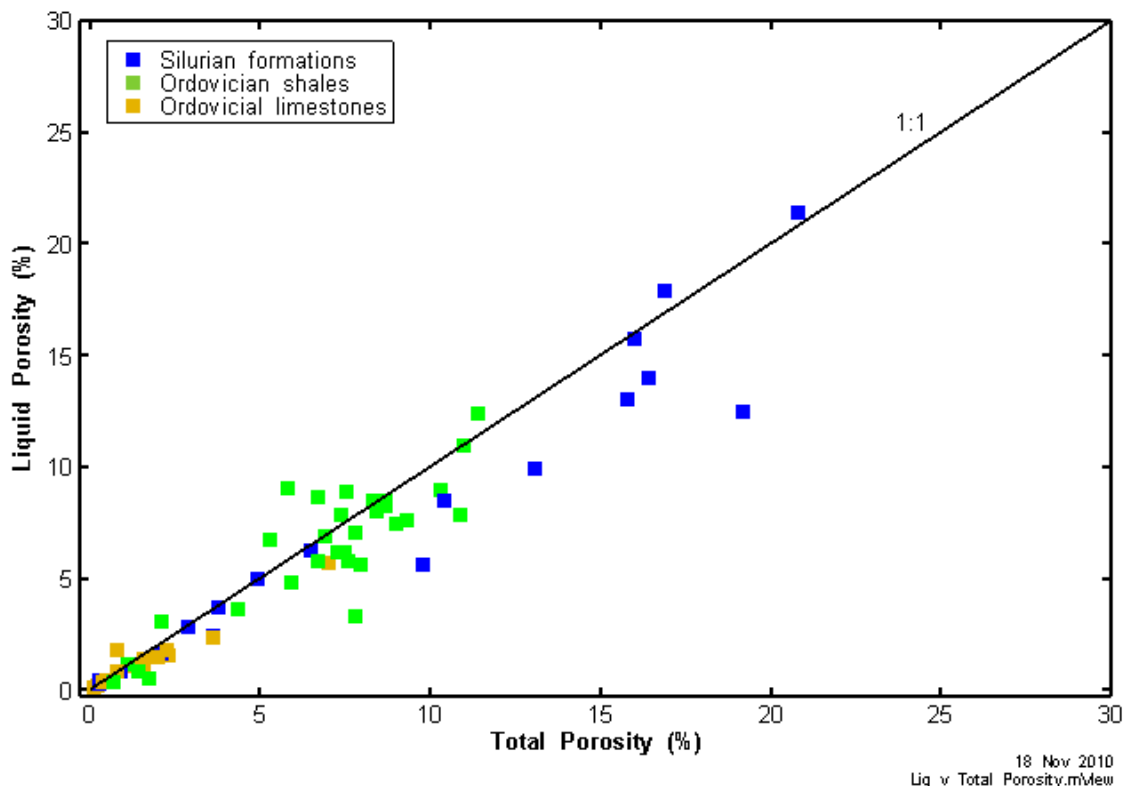


Figure 5 Comparison of Total and Liquid Porosity Measured by Core Labs on the Same DGR Core Plugs

Some of the observed differences in total porosity between different testing labs may also be due to the effects of imposing a confining stress during the testing of total porosity by Core Labs, which may result in a lower total porosity value due to microcrack closure. The Core Labs testing of total porosity for confined and unconfined DGR-3 and DGR-4 samples allows quantitative assessment of this effect. Figure 6 shows the ratio of unconfined to confined total porosity plotted by major formation groupings versus confined total porosity. This figure, which also shows mean ratio values for major groups of formations, indicates that core relaxation results in total porosity increases of about 17%, 31% and 39% for Silurian formations, Ordovician shales and Ordovician limestones, respectively, with the percentage change increasing with decreasing total porosity.

In addition, for the very low porosity Ordovician limestones, small errors in measurement procedures may significantly affect calculations of total and liquid porosities (i.e., such that the actual difference between total and liquid porosity may be smaller than the typical measurement error). Measurement error will be different for each analytical method and may include loss or gain of water during handling and testing due to evaporation and condensation, and the sensitivity and accuracy of measurements of water volumes and weights.

Although the porosity data inherently contains some measurement error and inconsistencies between samples and lab methodologies, the lower liquid porosity values compared to the total porosity that is evident in approximately 80 to 90% of the Ordovician limestone and Ordovician shale “hard bed” samples, and approximately 60% of the Devonian, Silurian, Ordovician shale, and Shadow Lake formations, indicates a gas phase is likely present.

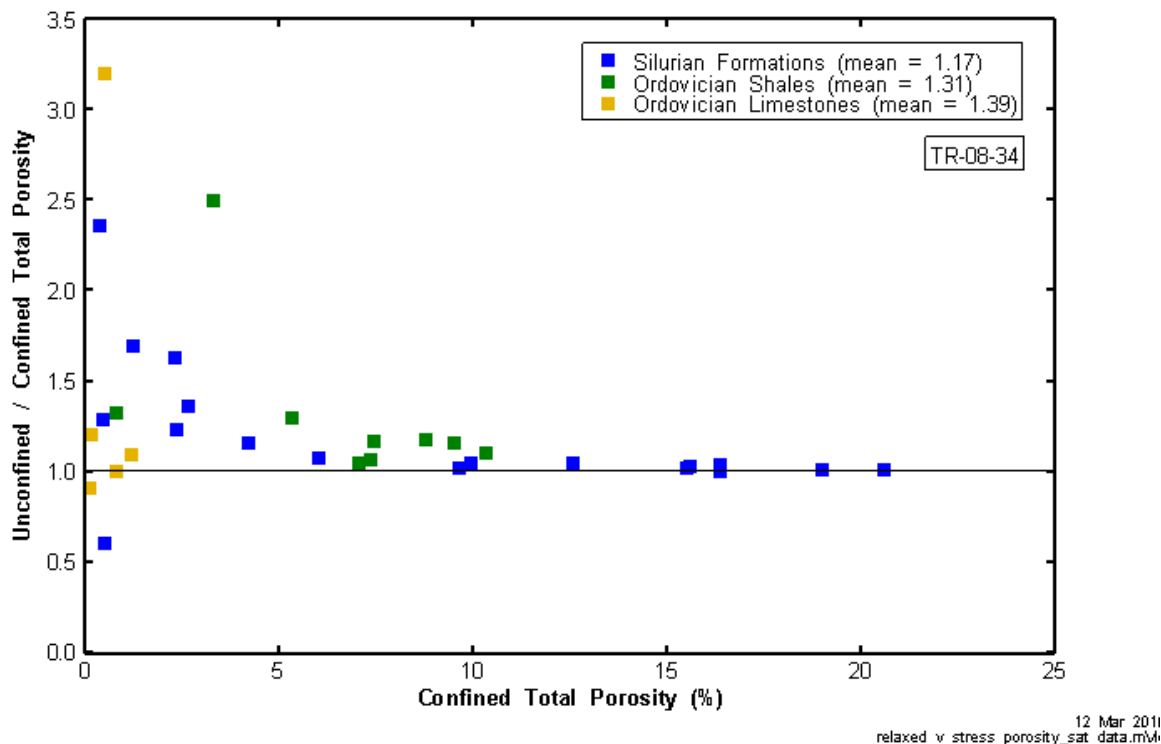


Figure 6 Comparison of ratio of unconfined to confined total porosity versus confined total porosity measured by Core Labs on DGR-3 and DGR-4 core plugs. Arithmetic mean ratios for major groups of formations are also shown.

3.2 Fluid Saturations

Core Labs, based in Houston, Texas, completed petrophysical testing on samples of core collected from boreholes DGR-2 to DGR-6 in accordance with TP-07-03, TP-08-11, TP-09-08 (Intera Engineering Ltd., 2007a, 2008b, and 2009c). These analyses provided (a) separate measurements of bulk density, permeability and porosity on “as received” and “clean and dry” core plugs, (b) mercury injection porosimetry and capillary pressure testing on the “clean and dry” core plugs, and (c) the estimation of fluid saturations of the core plugs primarily by Dean-Stark analysis.

3.2.1 Definitions and Experimental Methods

Fluid saturations (S) are defined in this report as the percentage (or fraction) of pore volume occupied by saline brine water (S_W), oil (S_O), and gas (S_G) in a sample of rock, where $S_W + S_O + S_G = 100\%$. Therefore brine water saturation (S_W) is the volume of brine water (V_b) divided by the total pore volume (V_p) (i.e., $S_W = V_b / V_p$). Samples analysed “as received” in the laboratory do not necessarily represent, but are assumed to approximate, in-situ conditions. Examples of measurements made on these samples include wet bulk density and liquid porosity. After the samples have all of their porewater and residual salts removed, they are referred to as “clean and dry” and are used for such measurements as dry bulk density and total porosity.

Dean Stark analysis is a distillation method used to directly determine the water content of a sample and also to indirectly determine its oil and gas contents, expressed as fluid saturations. Dean Stark analysis methods were developed within the oil and gas industry for petroleum reservoir characterization and were primarily developed to measure fluid saturations on samples with a relatively high (>5%) water content; however, the concepts of the experimental method are applicable for the DGR data.

Core samples of 76 mm diameter were collected for petrophysical testing during diamond coring of all DGR boreholes at the Bruce nuclear site during both Phase 1 and 2. All core samples were preserved in accordance with the general preservation and handling requirements of TP-06-10 for Phase 1 (Intera Engineering Ltd., 2007b), TP-08-04 for Phase 2A (Intera Engineering Ltd., 2008c), and TP-09-08 for Phase 2B (Intera Engineering Ltd., 2009c). As such, all samples were vacuum sealed within nitrogen flushed polyethylene and aluminum bags following core retrieval.

Core Labs drilled core plug sub-samples (5.1 x 3.8 cm) along the vertical axis from the DGR whole core samples provided by Intera, using humidified nitrogen as the bit lubricant. After being drilled and shaped into right cylinders, samples were submitted for analysis of basic rock properties (bulk density, permeability and pore volume measurements) and Dean Stark fluid saturations on the “as-received” samples.

Core Labs completes Dean Stark fluid saturation measurements using toluene as the solvent, which is heated, and the distilled water removed from the sample is condensed into a calibrated trap where the volume is directly measured. Core plug weights are measured at each step of the process. Following removal of distilled water, toluene is used as a reflux solvent to remove residual oil and the sample is re-weighed. Any salts remaining in the sample from evaporation during distillation are extracted by refluxing methanol. The sample was then dried (i.e., now “clean and dry”) and the pore volume was measured by the Boyle’s Law gas expansion method to yield the total porosity (TP-07-03 and TP-08-11) under a net confining stress of 17 kPa/m (DGR-2), 34 kPa/m (DGR-3 and DGR-4) and 0 kPa/m (DGR-5 and DGR-6).

3.2.2 Fluid Saturation Values

Core Labs estimated fluid saturations by the Dean Stark method (using total porosity measured on confined core plugs from DGR-2, DGR-3 and DGR-4, and unconfined core plugs from DGR-5 and DGR-6), as well as by NMR/He methods on unconfined core samples (DGR-4, DGR-5 and DGR-6). Core Labs completed these measurements on a total of 83 core samples, including 27 Dean Stark analyses from DGR-2 (20 vertically oriented and 7 horizontally oriented core plugs), 24 Dean Stark analyses from DGR-3 (24 vertical plugs), 13 Dean Stark analyses from DGR-4 (13 vertical plugs with 3 vertical plugs also analysed by NMR), 10 Dean Stark and 10 NMR analyses on the same core samples from DGR-5 (10 vertical plugs) and 9 Dean Stark and 9 NMR analyses on the same core samples from DGR-6 (9 vertical plugs).

The measured water and oil saturations are reported in Table 5 (DGR-2), Table 6 (DGR-3), Table 7 (DGR-4), Table 8 (DGR-5) and Table 9 (DGR-6) as the percentage of the pore volume (V_p) of the core plug occupied by water (S_w) or oil (S_o), respectively, along with the estimated gas saturations (S_g) that are computed as the residual of the pore volume (i.e., $S_g = 100 - S_w - S_o$).

Tables 5 to 9 list the DGR sample identifier (including sample depth as metres length below ground surface, mLBS), the formation from which the samples were recovered, and corresponding fluid saturations of the samples selected for petrophysical testing. Only the vertically-oriented DGR-2 samples are listed in Table 5 because there is some evidence that the horizontally-oriented DGR-2 core plugs, that were tested 3 months following collection, dried out during storage (TR-07-18). Similarly, all DGR-3 to DGR-6 results are based upon core plugs that were drilled from the core samples in a vertical direction relative to the bedding plane.

Figure 7 shows the water and gas fluid saturations, and Figure 8 shows the oil saturations, all determined by Dean Stark analysis as a profile with depth against the reference stratigraphy present at DGR-1 and DGR-2. DGR-3 to DGR-6 depths are adjusted to appear at the correct positions relative to DGR-1/2 stratigraphy.

Table 5 Dean Stark Fluid Saturations for DGR-2 Core Samples

Sample Identifier	Formation	Formation Group	Fluid Saturations (as percent of pore volume)			Total Porosity (%)
			Oil	Brine Water	Gas	
DGR2-457.66	Queenston	Upper Ordovician Shales	0.0	83.4	16.6	6.5
DGR2-488.51	Queenston		0.0	88.6	11.4	3.2
DGR2-515.01	Queenston		0.0	71.1	28.9	6.9
DGR2-540.00	Georgian Bay		0.0	89.9	10.1	0.4
DGR2-556.33	Georgian Bay		0.0	90.0	10.0	3.0
DGR2-576.09	Georgian Bay		0.0	93.2	6.8	7.2
DGR2-596.09	Georgian Bay		0.0	97.6	2.4	6.3
DGR2-613.93	Georgian Bay		0.0	73.5	26.5	7.0
DGR2-633.41	Blue Mountain		0.0	96.0	4.0	5.7
DGR2-650.12	Blue Mountain		0.0	101.7	-1.7	5.4
DGR2-658.88	Collingwood		0.0	69.7	30.3	1.3
DGR2-669.10	Cobourg	Middle Ordovician Limestones	0.0	101.0	-1.0	0.7
DGR2-678.63	Cobourg		0.0	106.8	-6.8	0.3
DGR2-687.10	Cobourg		0.0	95.4	4.6	1.1
DGR2-696.05	Sherman Fall		0.0	79.2	20.8	1.1
DGR2-706.77	Sherman Fall		0.0	88.3	11.7	1.3
DGR2-744.86	Kirkfield		0.0	77.4	22.6	1.2
DGR2-795.04	Gull River		0.0	81.9	18.1	0.4
DGR2-818.61	Gull River		0.0	91.3	8.7	1.6
DGR2-845.96	Cambrian	Cambrian	0.0	96.7	3.3	4.3

Table 6 Dean Stark Fluid Saturations for DGR-3 Core Samples

Sample Identifier	Formation	Formation Group	Fluid Saturations (as percent of pore volume)			Total Porosity (%)
			Oil	Brine Water	Gas	
DGR3-200.50	Salina F Unit	Silurian	0.0	82.2	17.8	12.6
DGR3-204.24	Salina F Unit		0.0	100.0	0.0	0.5
DGR3-230.47	Salina F Unit		0.0	98.7	1.3	10.0
DGR3-251.68	Salina E Unit		0.0	100.0	0.0	16.4
DGR3-270.49	Salina C Unit		0.0	99.8	0.2	25.0
DGR3-291.57	Salina B Unit		0.0	100.0	0.0	16.4
DGR3-308.53	Salina A2 carbonate		0.0	100.0	0.0	15.6
DGR3-334.81	Salina A2 evaporite		1.4	85.5	14.5	15.5
DGR3-380.68	Salina A1 evaporite		0.0	78.4	21.6	0.5
DGR3-385.82	Salina A0		0.0	90.7	9.3	2.7
DGR3-398.05	Goat Island		0.0	83.6	16.4	0.5
DGR3-408.41	Goat Island		0.0	100.0	0.0	2.3
DGR3-452.76	Manitoulin		0.0	82.9	15.7	0.4
DGR3-477.90	Queenston		Upper Ordovician Shales	0.0	92.2	7.8
DGR3-496.54	Queenston	0.0		100.0	0.0	7.5
DGR3-521.05	Queenston	0.0		100.0	0.0	7.4
DGR3-565.40	Georgian Bay	0.0		100.0	0.0	10.3
DGR3-585.89	Georgian Bay	0.0		100.0	0.0	8.8
DGR3-629.11	Blue Mountain	0.0		96.3	3.7	9.5
DGR3-656.92	Blue Mountain	0.0		100.0	0.0	0.8
DGR3-673.14	Cobourg	Middle Ordovician Limestones	0.0	100.0	0.0	0.1
DGR3-755.38	Kirkfield		0.0	100.0	0.0	0.5
DGR3-776.82	Coboconk		0.0	92.0	8.0	0.2
DGR3-814.66	Gull River		0.0	85.4	14.6	1.2

Table 7 Dean Stark Fluid Saturations for DGR-4 Core Samples

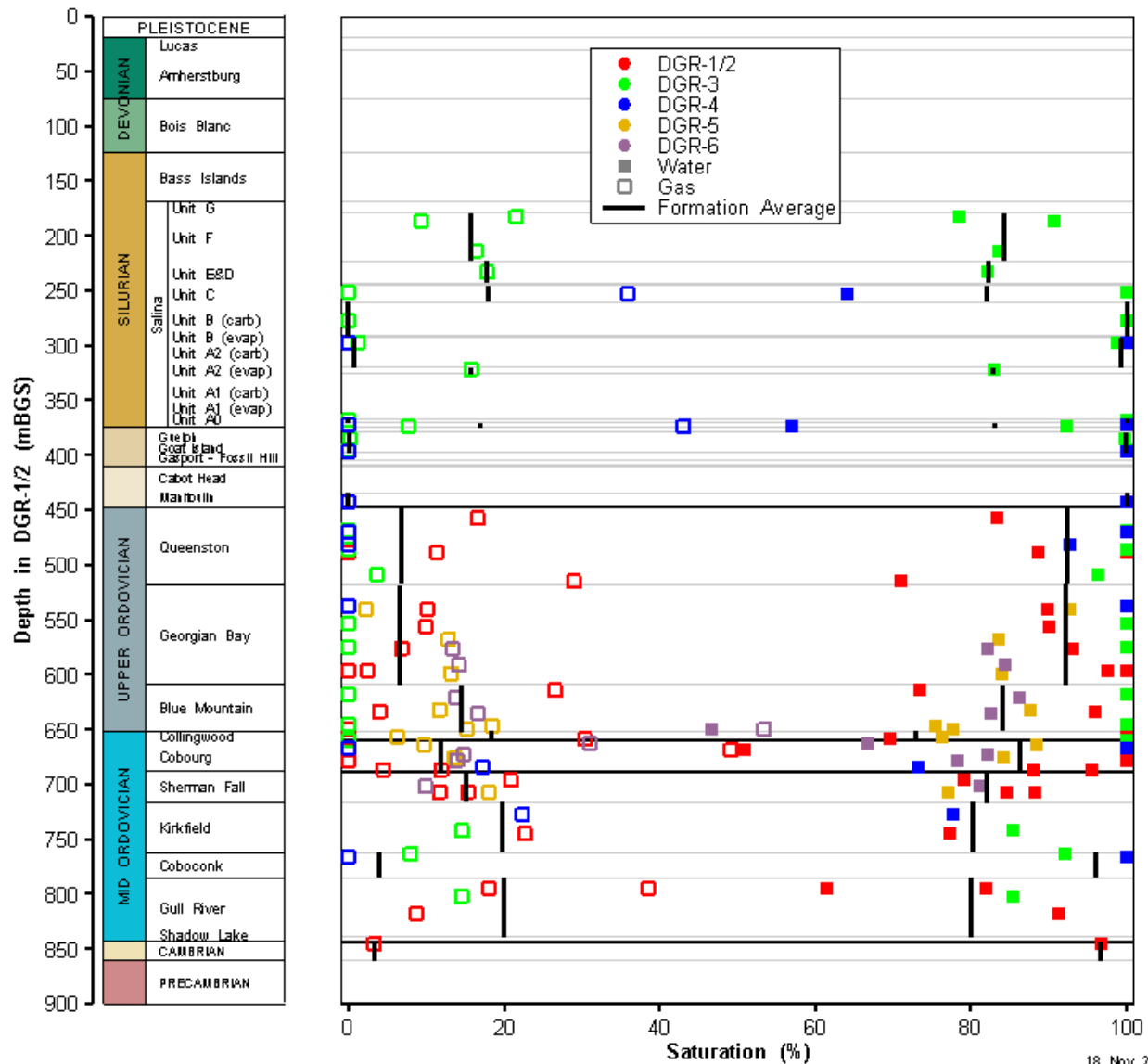
Sample Identifier	Formation	Formation Group	Fluid Saturations (as percent of pore volume)			Total Porosity (%)
			Oil	Brine Water	Gas	
DGR4-255.08	Salina C Unit	Silurian	0.0	64.1	35.9	19.0
DGR4-296.97	Salina A2 Unit		0.0	100.0	0.0	6.1
DGR4-373.63	Salina A0 Unit		0.0	100.0	0.0	2.4
DGR4-375.40	Salina A0 Unit		0.0	57.0	43.0	9.7
DGR4-398.63	Goat Island		0.0	100.0	0.0	1.2
DGR4-441.78	Cabot Head		0.0	100.0	0.0	4.2
DGR4-468.92	Queenston	Upper Ordovician Shales	0.0	100.0	0.0	5.3
DGR4-481.50	Queenston		7.3	92.7	0.0	8.6
DGR4-538.65	Georgian Bay		0.0	100.0	0.0	3.3
DGR4-668.89	Cobourg	Middle Ordovician Limestones	0.0	99.8	0.2	0.8
DGR4-685.30	Cobourg		9.5	73.2	17.3	2.1
DGR4-728.62	Kirkfield		0.0	77.6	22.4	1.3
DGR4-767.65	Coboconk		0.0	100.0	0.0	0.8

Table 8 Dean Stark Fluid Saturations for DGR-5 Core Samples

Sample Identifier	Formation	Formation Group	Fluid Saturations (as percent of pore volume)			Total Porosity (%)
			Oil	Brine Water	Gas	
DGR5-583.69	Georgian Bay	Upper Ordovician Shales	5.0	92.7	2.3	1.4
DGR5-612.31	Georgian Bay		3.6	83.5	12.9	10.9
DGR5-643.19	Georgian Bay		2.7	84.0	13.3	9.0
DGR5-678.52	Blue Mountain		0.7	87.6	11.7	9.3
DGR5-695.00	Blue Mountain		6.0	75.4	18.6	8.0
DGR5-697.54	Blue Mountain		7.0	77.8	15.2	7.6
DGR5-705.36	Collingwood	Middle Ordovician Limestones	17.4	76.3	6.3	1.8
DGR5-712.74	Cobourg		1.8	88.5	9.7	2.0
DGR5-725.11	Cobourg		2.1	84.2	13.7	3.6
DGR5-757.54	Sherman Fall		4.8	77.1	18.0	2.3

Table 9 Dean Stark Fluid Saturations for DGR-6 Core Samples

Sample Identifier	Formation	Formation Group	Fluid Saturations (as percent of pore volume)			Total Porosity (%)
			Oil	Brine Water	Gas	
DGR6-647.39	Georgian Bay	Upper Ordovician Shales	4.4	82.1	13.4	7.5
DGR6-664.58	Georgian Bay		1.4	84.4	14.1	7.3
DGR6-699.62	Blue Mountain		0.1	86.1	13.8	6.7
DGR6-717.68	Blue Mountain		0.7	82.6	16.7	5.9
DGR6-736.57	Blue Mountain		0.0	46.6	53.4	0.7
DGR6-750.55	Cobourg	Middle Ordovician Limestones	2.3	66.7	31.0	0.5
DGR6-762.01	Cobourg		3.1	82.1	14.9	0.4
DGR6-768.31	Cobourg		7.8	78.3	13.9	0.5
DGR6-797.31	Sherman Fall		9.1	81.0	9.9	7.0



18 Nov 2010
 PoreFl sat profile.mView

Figure 7 Profile of Water and Gas Saturations in DGR Cores

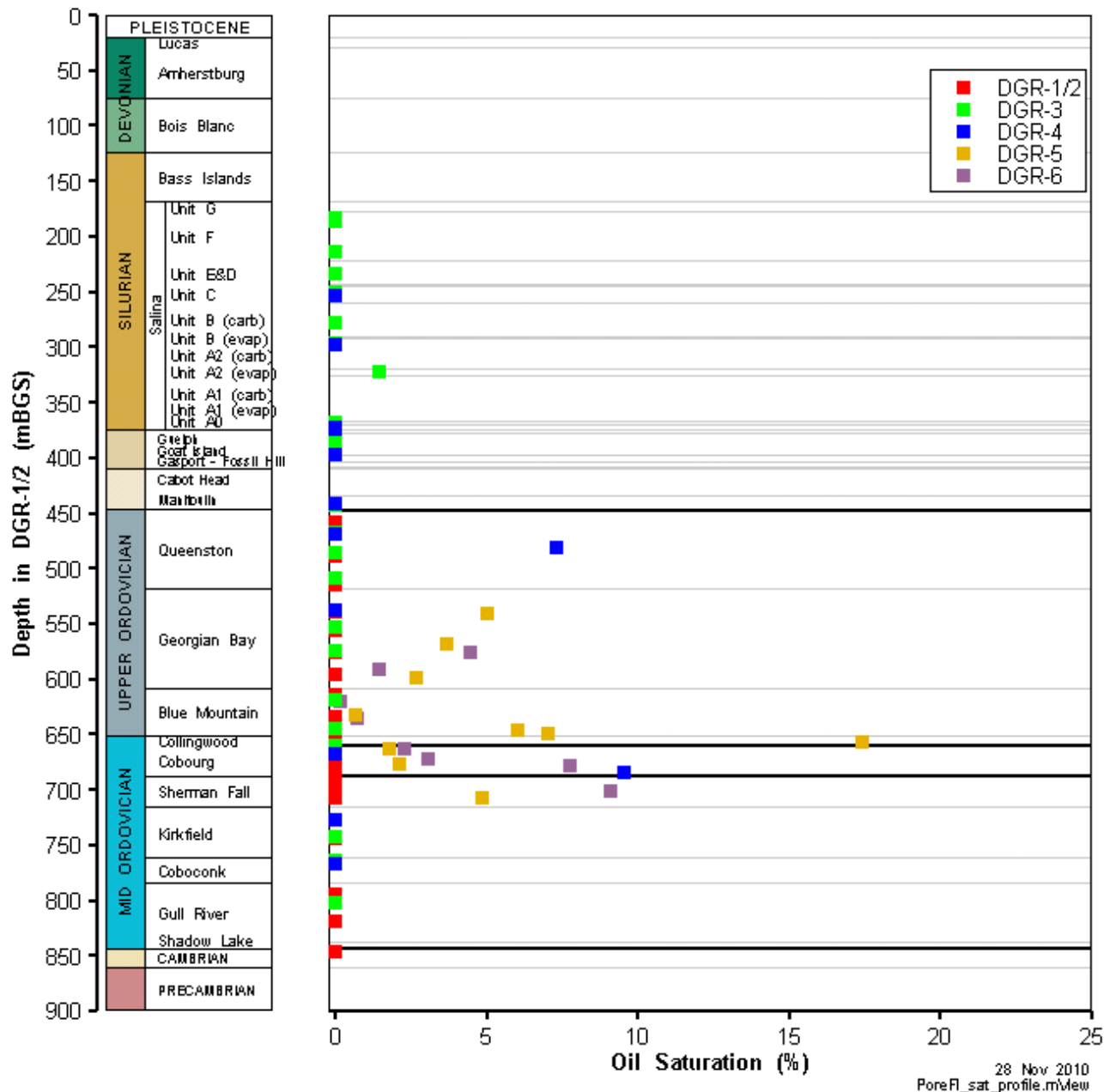


Figure 8 Profile of Oil Saturations in DGR Cores

The relative oil and water saturations originally reported by Core Labs were based on several assumptions concerning oil and pore fluid properties, including: [1] the oil density is assumed to be 0.83 g/cc, similar to other oils in southwestern Ontario, and [2] the porewater (i.e., brine) density (ρ_b) and salinity (S) are assumed to be 1088 kg/m³ and 50,000 mg/kg, respectively, regardless of depth. The data presented in this Technical Report have been further corrected by assuming formational average values for brine density and brine mass fraction of salts, based on total dissolved solids (TDS) concentrations. The methodology for correcting the water saturation data includes reducing the volume of brine water used in the brine water saturation calculation ($S_w = V_b/V_p$) to a volume of pure water, and then converting it to the corrected volume of brine based on formational average fluid properties as described in Equation [2] (Section 3.1.2).

Tables 5 to 9 and Figures 7 and 8 show that the range of estimated oil saturations is 0 to 17.4% with 63 of the 83 core plugs showing 0% oil saturation. The limited and sporadic occurrence of oil saturation in DGR cores is supported by core observations, as described during drilling, including a thin section of the Salina A1 Unit carbonate and parts of the Coboconk and Gull River formation limestones, as well as petroliferous odours in several Ordovician shale and limestone formations. However, because the petrophysical testing program primarily focused on characterization of the properties of the Ordovician and other low permeability barrier rocks, and oil presence was limited in these formations, direct comparison of oil saturations determined from fluid saturation testing and core observations was not possible with available core data.

Additional graphical results are presented with water saturations (Figure 9) and the computed gas saturations (Figure 10) plotted against total porosity for various groups of formations. The mean \pm standard deviation for the 83 samples shown in the two figures are $S_w = 95.6 \pm 30.5\%$ (Figure 9) and $S_g = 10.9 \pm 12.0\%$ (Figure 10). There appears to be no correlation between the water saturation and total porosity in that many porous Silurian samples (mean total porosity = 8.2%) contain similar water saturations as the much less porous Middle Ordovician limestones (mean total porosity = 1.4%), while the Upper Ordovician shales are grouped in the middle (mean total porosity = 6.3%).

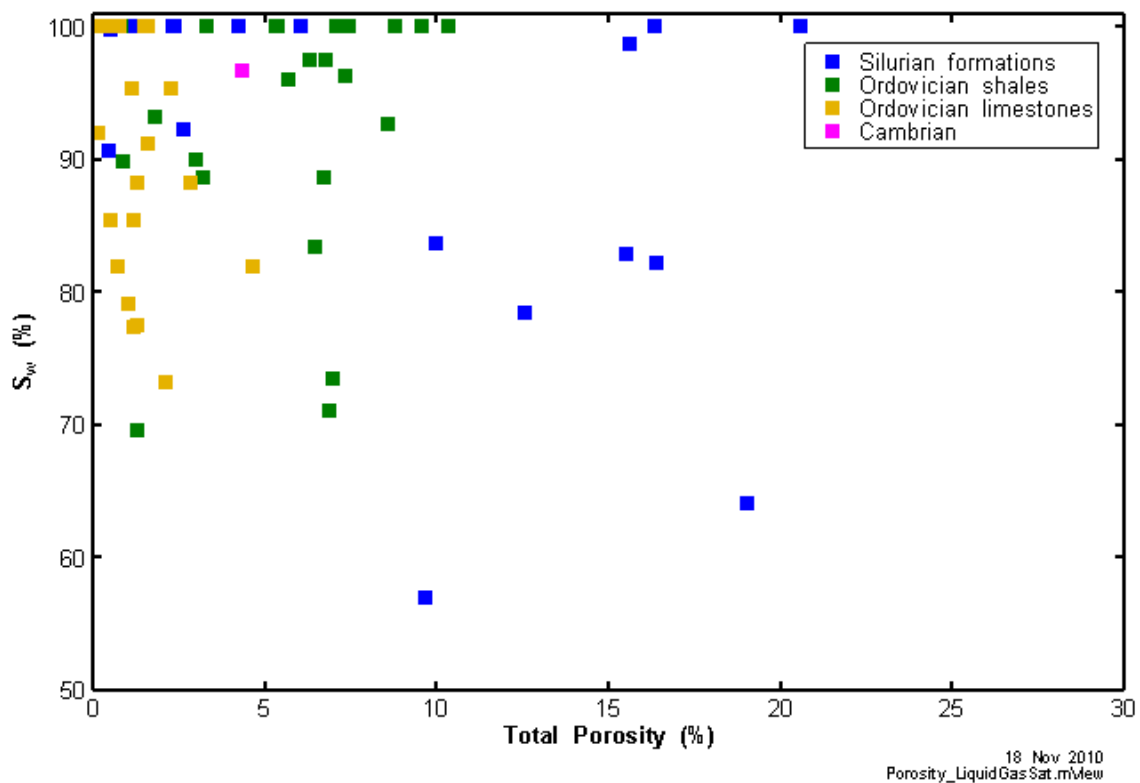


Figure 9 Water Saturations (S_w) for DGR-2, DGR-3, DGR-4, DGR-5 and DGR-6 Cores Plotted Against Their Total Porosity

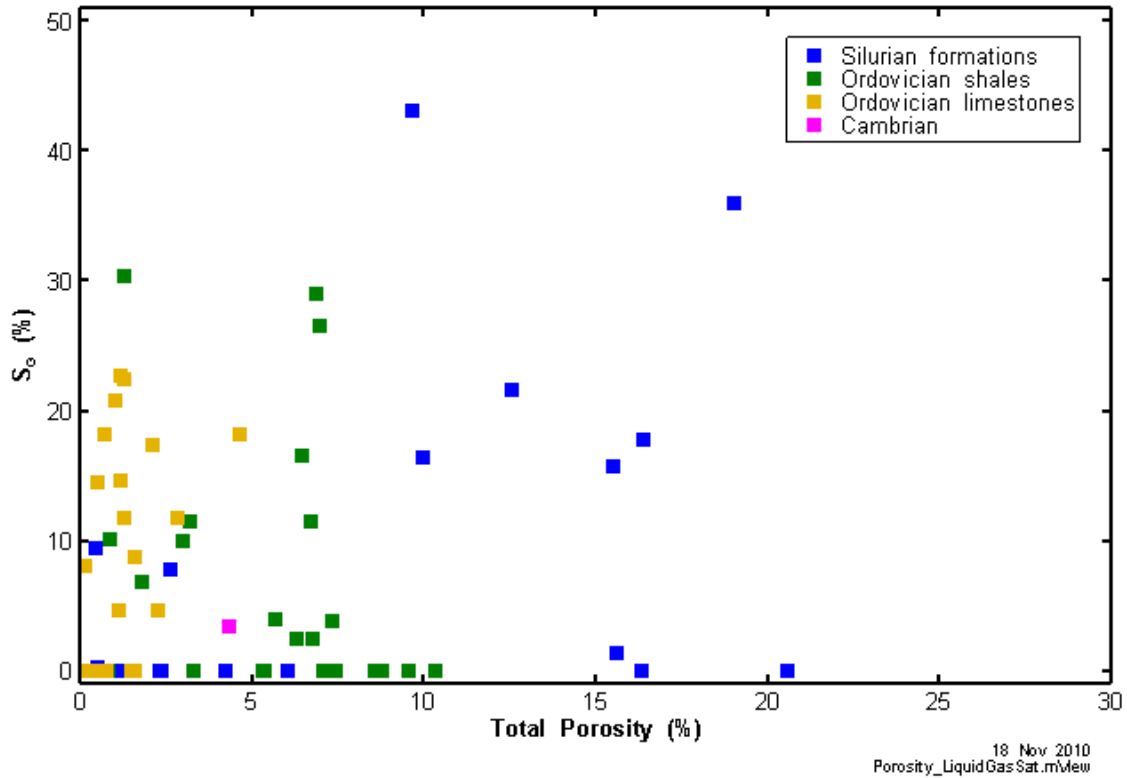


Figure 10 Gas Saturations (S_G) for DGR-2, DGR-3, DGR-4, DGR-5 and DGR-6 Cores Plotted Against Their Total Porosity

3.2.3 Assessment of Fluid Saturation Data

The Dean Stark results and total porosity measurements (determined by Boyle’s Law) suggest that there is a residual fraction of the pore volume in which a gas phase is likely present (i.e., $S_G > 0$). This value varies from 0% to nearly 50%.

In order to understand the uncertainty in these values that are calculated from direct measurements of water yield from the core plug (V_W) per unit pore volume (V_P), the analytical uncertainty in V_W and V_P must be determined. The error in determining V_W is ~ 50 μ L, while the error in total porosity measurement is 0.3%. The fractional uncertainty in S_w vs. fractional porosity for DGR cores is given in Woodhouse (1998) using error propagation theory:

$$\frac{dS_w}{S_w} = \sqrt{\left(\frac{dV_w}{V_w}\right)^2 + \left(\frac{dV_p}{V_p}\right)^2} \quad [4]$$

Figure 11 shows the fractional uncertainty in S_w vs. total porosity for DGR samples. For porosities <3%, in particular the Ordovician limestones and carbonate-rich units in the Silurian formations and Upper Ordovician shales, there is a significant error that typically exceeds 20% in S_w (i.e., $dS_w/S_w > 0.2$).

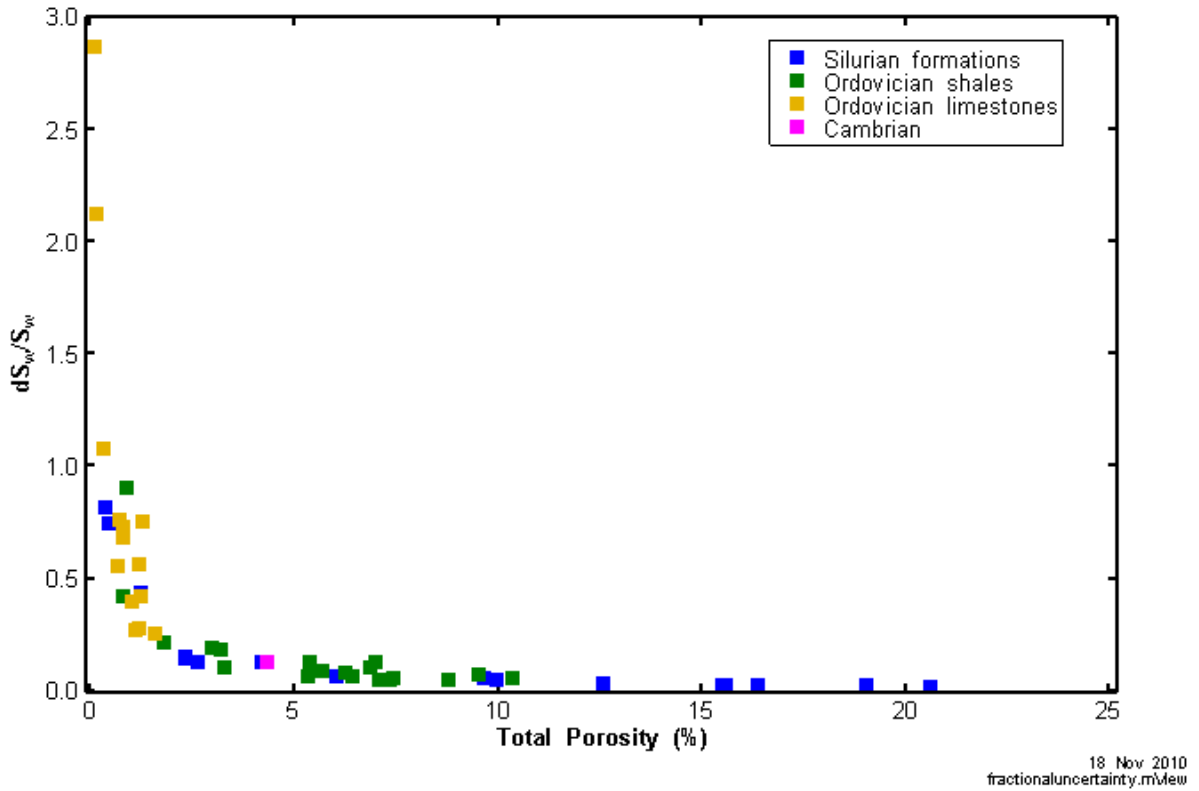


Figure 11 Fractional Uncertainty in the Water Saturation vs. Total Porosity in DGR Cores

Five of the twelve samples shown in Figure 11 that exceed 50% uncertainty (i.e., $dS_w/S_w > 0.5$) are Cobourg Formation limestones. This elevated uncertainty in the carbonate rocks is because the error in estimating the water yield from the Dean Stark method is $\sim 50 \mu\text{L}$ and the low water yields associated with the carbonate rock samples produce large uncertainties. Clearly, carbonate mineral cementation, sulphate mineral precipitation, and compaction of the rock column have caused a major reduction in porosity during the Paleozoic that is consistent with the great age of these rocks (Lucia, 1999, pp.109-119).

In order to verify the estimates from the Dean Stark extractions, Nuclear Magnetic Resonance (NMR) analysis of core plugs was undertaken to measure the total liquid saturation ($S_L = S_w + S_o$) on 22 core samples (3 from DGR-4, all 10 from DGR-5 and all 9 from DGR-6), and the gas saturation (S_g) was estimated on the same core plug by Boyle's Law gas expansion using $\text{He}_{(g)}$. These values are presented in Table 10 and Figure 12, together with the estimates of liquid and gas saturations by Dean Stark extractions.

The correlation between the two sets of data for both the shale and two limestone samples is good ($r^2=0.94$) and indicates that the Dean Stark derived estimates of S_g appear representative of in-situ conditions (noting the limitation of this methodology concerning low porosity carbonates mentioned above).

Table 10 NMR and Dean Stark Fluid Saturations for DGR-4, DGR-5 and DGR-6 Core Samples (%)

<i>Sample Identifier</i>	<i>Formation</i>	<i>NMR Liquid Saturation</i>	<i>He Gas Saturation</i>	<i>Dean Stark Liquid Saturations¹</i>	<i>Dean Stark Gas Saturation</i>	<i>Total porosity²</i>
Shales						
DGR4-481.50	Queenston	86.4	13.6	92.0	8.0	8.6
DGR5-583.69	Georgian Bay	78.3	21.7	97.7	2.3	1.4
DGR5-612.31	Georgian Bay	92.6	7.4	87.1	12.9	10.9
DGR5-643.19	Georgian Bay	96.4	3.6	86.7	13.3	9.0
DGR5-678.52	Blue Mountain	98.1	1.9	88.3	11.7	9.3
DGR5-695.00	Blue Mountain	94.9	5.1	81.4	18.6	8.0
DGR5-697.54	Blue Mountain	96.8	3.2	84.8	15.2	7.6
DGR6-647.39	Georgian Bay	90.6	9.4	86.6	13.4	7.5
DGR6-664.58	Georgian Bay	87.3	12.7	85.9	14.1	7.3
DGR6-699.62	Blue Mountain	89.8	10.2	86.2	13.8	6.7
DGR6-717.68	Blue Mountain	84.9	15.1	83.3	16.7	5.9
DGR6-736.57	Blue Mountain	60.9	39.1	46.6	53.4	0.7
Limestones						
DGR4-685.30	Cobourg	65.4	34.6	74.0	26.0	2.1
DGR4-728.62	Sherman Fall	76.9	23.1	76.0	24.0	1.3
DGR5-705.36	Collingwood	83.6	16.4	93.7	6.3	1.8
DGR5-712.74	Cobourg	92.6	7.4	90.3	9.7	2
DGR5-725.11	Cobourg	96.1	3.9	86.3	13.7	3.6
DGR5-757.54	Sherman Fall	96.3	3.7	82.0	18.0	2.3
DGR6-750.55	Cobourg	77.9	22.1	69.0	31.0	0.5
DGR6-762.01	Cobourg	85.2	14.8	85.1	14.9	0.4
DGR6-768.31	Cobourg	83.4	16.6	86.1	13.9	0.5
DGR6-797.31	Sherman Fall	95.1	4.9	90.1	9.9	7

¹ salinities assumed as formational averages presented in Table 2.

² total porosity measured under confining stress for DGR-4 samples and under ambient conditions for DGR-5 and DGR-6 samples

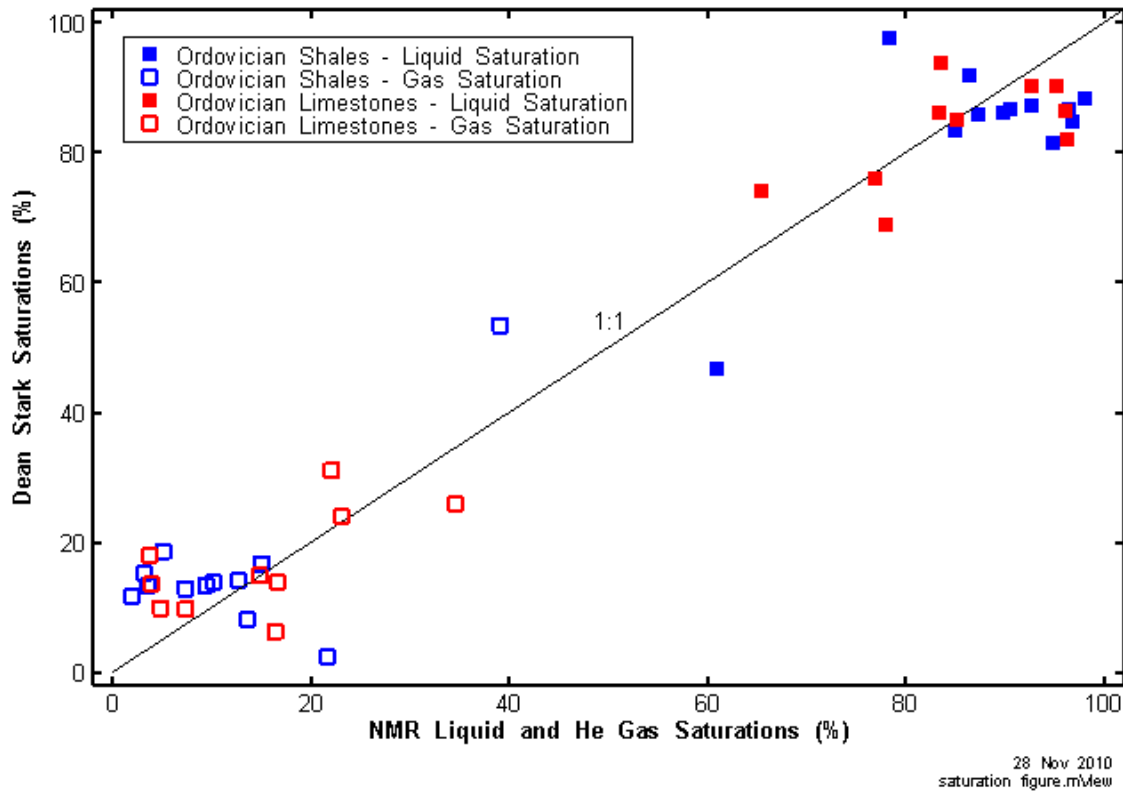


Figure 12 Comparison of Methods of Measuring Fluid Saturations in DGR-4 cores

Table 11 summarizes the fluid saturation data by groups of formations and includes the arithmetic mean, standard deviation, and total number of samples.

Table 11 Summary of Fluid Saturation Values by Formation Grouping

Formation Group	Count	Oil Saturation (S_o)		Brine Water Saturation (S_w)		Gas Saturation (S_g)	
		Mean	St. Dev	Mean	St. Dev	Mean	St. Dev
Silurian and Devonian	19	0.1	0.3	91.0	13.1	8.9	13.1
Ordovician shales	26	1.3	2.3	90.3	9.7	8.4	8.9
Ordovician shale hard beds	7	0.7	1.9	86.8	18.4	12.5	18.7
Ordovician limestones	30	1.9	0.3	84.3	12.2	13.9	11.7
Shadow Lake and Cambrian sandstone	1	0	0	96.7	0	3.3	0

Therefore, petrophysical testing indicates the likelihood that there is a significant gas phase present in the Paleozoic rocks beneath the Bruce nuclear site. The gas saturations in the Silurian and Devonian formations and the Upper Ordovician shales have mean and standard deviation values of $S_g = 8.9 \pm 13.1\%$ (Silurian and Devonian) and $8.4 \pm 8.9\%$ (Ordovician shales). The values for the Ordovician shale hard beds and limestones are somewhat higher with values of $12.5 \pm 18.7\%$ (Ordovician hardbeds) and $13.9 \pm 11.7\%$ (Ordovician limestones). Only one sample was tested from the Cambrian sandstone and it had a calculated gas saturation

of 3.3%. These gas saturations are considerably lower than those exploited commercially in shale-gas reservoirs in North America in which $S_G > 40\%$ (Curtis, 2002). Some shales, however, such as the Pierre shale in South Dakota, as reported by Neuzil (1993, p. 2008), had measured $S_W \sim 100\%$ (i.e., $S_G \sim 0\%$) despite the low fluid pressures in this shale.

4 Geochemical Data

4.1 Geochemical Partitioning of Gas - Experimental Methods

Abnormally low fluid pressures have been measured in the DGR boreholes (TR-08-31, Geofirma Engineering Ltd., 2011d). A possible causal mechanism for these pressures is unloading associated with glacial erosion and ice-sheet retreat. As suggested by Neuzil and Pollock (1982), this would cause degassing of the pore fluid into newly created pore space and the establishment of a gas phase. The likelihood of this occurring is evaluated by considering the possibility of a methane-carbon dioxide gas phase in the pore spaces of the DGR Paleozoic sequence of rocks.

Extraction of pore waters by vacuum distillation methods at the University of Ottawa (TP-08-10, Intera Engineering 2008d) is accompanied by release of both carbon dioxide (CO_2) and methane (CH_4) from the rock. These distillates are then measured for both total quantities of gas and stable isotopes of oxygen (O), carbon (C) and hydrogen (H). The methane and carbon dioxide concentrations measured in the pore water were calculated by dividing the mass of methane and carbon dioxide released from a rock sample by the amount of water released from the same sample (TR-07-21, TR-08-19). This calculation assumes that the extraction principally releases methane and carbon dioxide from pore water and from any separate gas phase that may be present. The methodology allows a convenient comparison of the pore water methane and carbon dioxide concentrations to the gas solubility. Methane and carbon dioxide concentrations that exceed the solubility limits suggest a separate gas phase is present.

The solubility of gas in water is affected by the type of gas, the solute concentration in the water, as well as the water temperature and water pressure. The high porewater solute concentrations and broad range of subsurface pressures measured at the Bruce nuclear site must be accounted for in any analysis of methane and carbon dioxide gas solubility.

The thermodynamic-based model developed by Duan and Mao (2006) calculates the solubility of methane and carbon dioxide at a range of solute concentrations, water temperatures and water pressures. Due to the complexity of ion-ion interactions at high solute concentrations, the Duan and Mao (2006) model assumes a binary solution, in this case sodium chloride (NaCl).

4.2 Methane and Carbon Dioxide Solubility Data

Methane and carbon dioxide solubility curves were calculated using the Duan and Mao (2006) model assuming a constant temperature of 25°C and three different formation pressures (2, 6 and 11 MPa). These pressures were measured in the Ordovician shales, the Cobourg Formation and the Cambrian, respectively, through hydraulic testing and groundwater monitoring using the Westbay MP55 systems at the Bruce nuclear site (Geofirma Engineering Ltd, 2011d).

Groundwater and porewater at the site are described as sodium-chloride (Na-Cl) and sodium/calcium-chloride (Na:Ca-Cl) type waters, which indicates sodium (Na) and chloride (Cl) are commonly the dominant ions in the porewater. However, calcium (Ca) can have significant concentrations (particularly in the Cambrian groundwater) and other ions are also present in the groundwater and porewater at the Bruce nuclear site (TR-07-21, TR-08-19).

Since the Duan and Mao (2006) model requires solute concentrations for binary salts (i.e., NaCl) the solute concentrations for porewaters at the Bruce nuclear site were estimated using the following two methods. The first method summed together the molality concentration of all cations and anions and divided the result by two. This method assumes all of the ions in solution have the same ion-gas interaction as Na and Cl with methane. Methane is more soluble with divalent cations than monovalent cations (Stoessel and Byrne, 1982); therefore, the type of anion, for example chloride and sulphate, has a small effect on the solubility of methane in water. This method assumes all cations behave like, and can be approximated as, monovalent sodium (Na^+) ions, which likely underestimates the solubility of methane because a solution with divalent cations such as calcium (Ca^{2+}) and magnesium (Mg^{2+}) would realistically allow more methane to dissolve compared to a solution consisting solely of monovalent cations such as sodium (Na^+).

The second method for estimating the equivalent NaCl concentration was to sum together the pore water Na and Cl concentrations and divide by two to calculate the NaCl concentration. This method underestimates the actual porewater solute concentrations and the first method presented above overestimates the NaCl concentrations. Together, these two methods show a range of NaCl concentrations for the Duan and Mao (2006) model input. This range of concentrations likely accounts for the true ion-methane interaction that occurs in the porewater at the Bruce nuclear site.

4.2.1 Methane Solubility

The methane solubility curves for NaCl concentrations were calculated for concentrations from 0 to 6 molal NaCl for pressures of 2, 6 and 11 MPa (Figures 13 and 14). Figures 13 and 14 show the porewater methane results with the NaCl concentrations calculated from DGR-3 (Figure 13) and DGR-4 (Figure 14) using the first method described above (all ions summed).

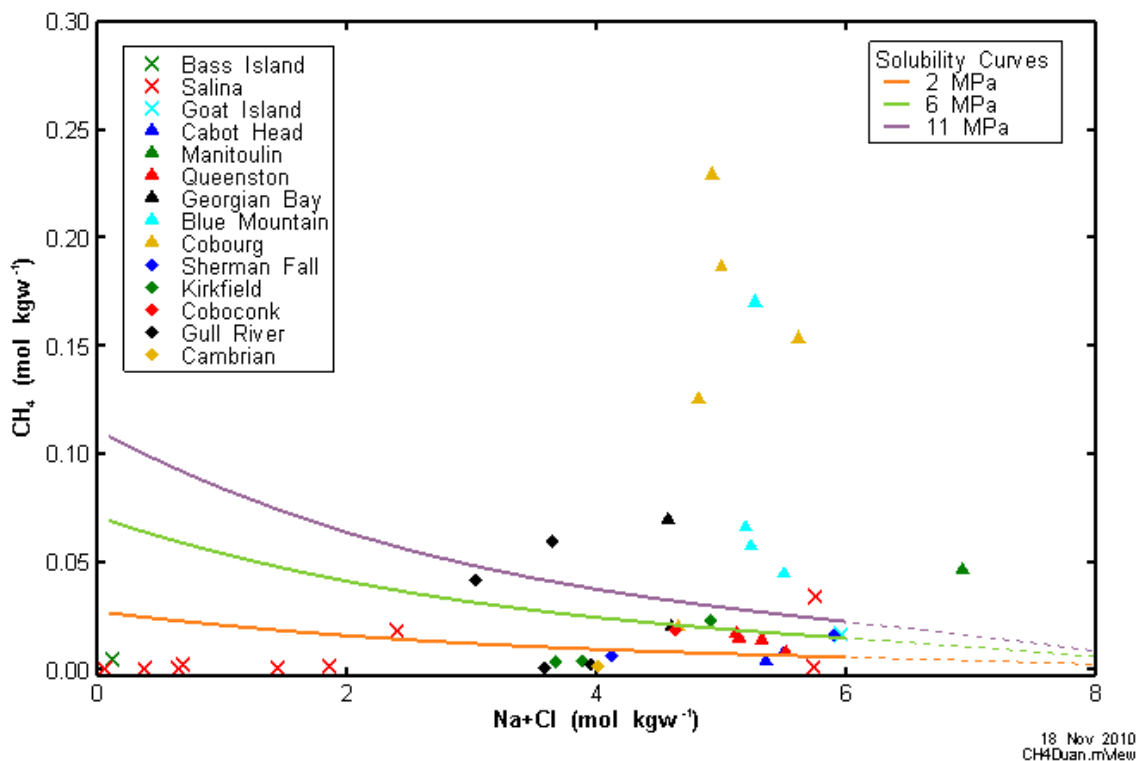


Figure 13 Cross Plot of Apparent CH₄ and Na+Cl Porewater Concentrations Compared to Calculated CH₄ Solubility in DGR-3

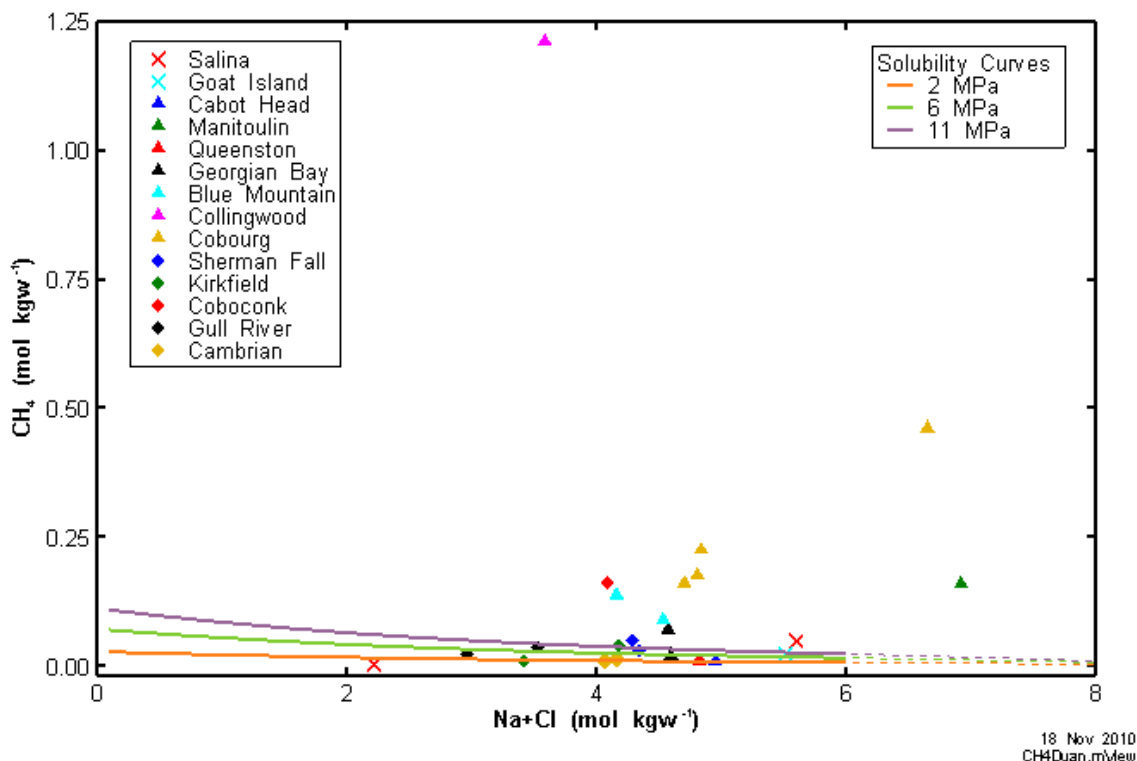


Figure 14 Cross Plot of Apparent CH₄ and Na+Cl Porewater Concentrations Compared to Calculated CH₄ Solubility in DGR-4

Duan and Mao (2006) report that the model is applicable to a maximum NaCl concentration of 6 molal for methane (CH₄) only. The dashed lines presented in Figures 13 and 14 are extrapolations of the calculated methane solubilities at each pressure above 6 molal. The solubility curves may not be applicable at these high molal concentrations due to ion-ion and ion-gas interactions.

Considering the errors in analysis and solubility calculations, it is difficult to confidently label samples with methane concentrations below the 11 MPa solubility curve as “super-saturated” for this initial analysis. Small errors in the thermodynamic model or laboratory analyses could adjust the relative position of the sample results from near the 6 MPa line to below the 2 MPa line. Even with this consideration there are several samples that plot above the methane solubility line. Methane concentrations above the 11 MPa solubility curve are primarily from the Collingwood/Cobourg and Blue Mountain formations with one to two samples from each of the Salina A1 Unit, Manitoulin, Georgian Bay, Kirkfield and Gull River formations.

These results suggest methane could be present in the Salina A1 Unit, the Manitoulin, the Georgian Bay, Blue Mountain, Collingwood, Cobourg, Coboconk, Sherman Fall and Kirkfield formations. This analysis does not account for methane adsorbed to organic carbon in the formations. Methane adsorption to organic carbon may be significant where high Total Organic Carbon (TOC) is present. However, methane is still likely present as a gas phase in the Collingwood Member, and possibly the Cobourg and Blue Mountain formations, as indicated by the position of data points clearly above the 11 MPa solubility curve in Figure 14. Additionally, a decrease in pore pressure may cause dissolved methane to exolve from the pore water.

4.2.2 Carbon Dioxide Solubility

Similarly, carbon dioxide solubility curves were calculated using the Duan and Sun (2003) model assuming a constant temperature of 25°C and three pressures (2, 6 and 11 MPa). The carbon dioxide model is only valid for

NaCl concentrations from 0 to 4.5 molal. Figures 15 and 16 show the porewater carbon dioxide results with the NaCl concentrations calculated from DGR-3 (Figure 15) and DGR-4 (Figure 16) using the first method described above (all ions summed).

The dashed lines in the figures represent the extrapolation of the thermodynamic model up to 6 molal NaCl. Molal NaCl concentrations were calculated as the summation of all of the anions and cations (both as molality) and divided by two, which is the same as the first method presented above. A comparison of the carbon dioxide concentrations in both DGR-3 and DGR-4 samples to the solubility limits show carbon dioxide has not exceeded the solubility limits. Therefore, a separate carbon dioxide (CO₂) gas phase is not likely present. However, a decrease in the pore pressure may result in the creation of a separate carbon dioxide phase.

These values exceed the measured fluid pressures at these depths (3-6 MPa in Cobourg Formation and Upper Ordovician shales) suggesting that a separate gas phase would form in the rock. Note that these methane concentrations must be considered as minimum values because possible losses during core recovery and storage prior to analysis are not accounted for. There is presently no method at the University of Ottawa to assess percent recovery of CH₄ from the cores during vacuum distillation.

CO₂ recovered during vacuum distillation offers a second line of evidence supporting a separate gas phase under in-situ conditions. CO₂ is recovered during vacuum distillation by freezing into septum vials along with water released as vapour during rock heating under vacuum. Amounts of CO₂, normalized to porewater mass, varying up to and exceeding 100 mmol/kgw, are measured. When considered as a dissolved gas phase and assuming that the porewaters are in equilibrium with calcite, the resulting in-situ pH of the pore fluids would be on the order of 4 to 4.5.

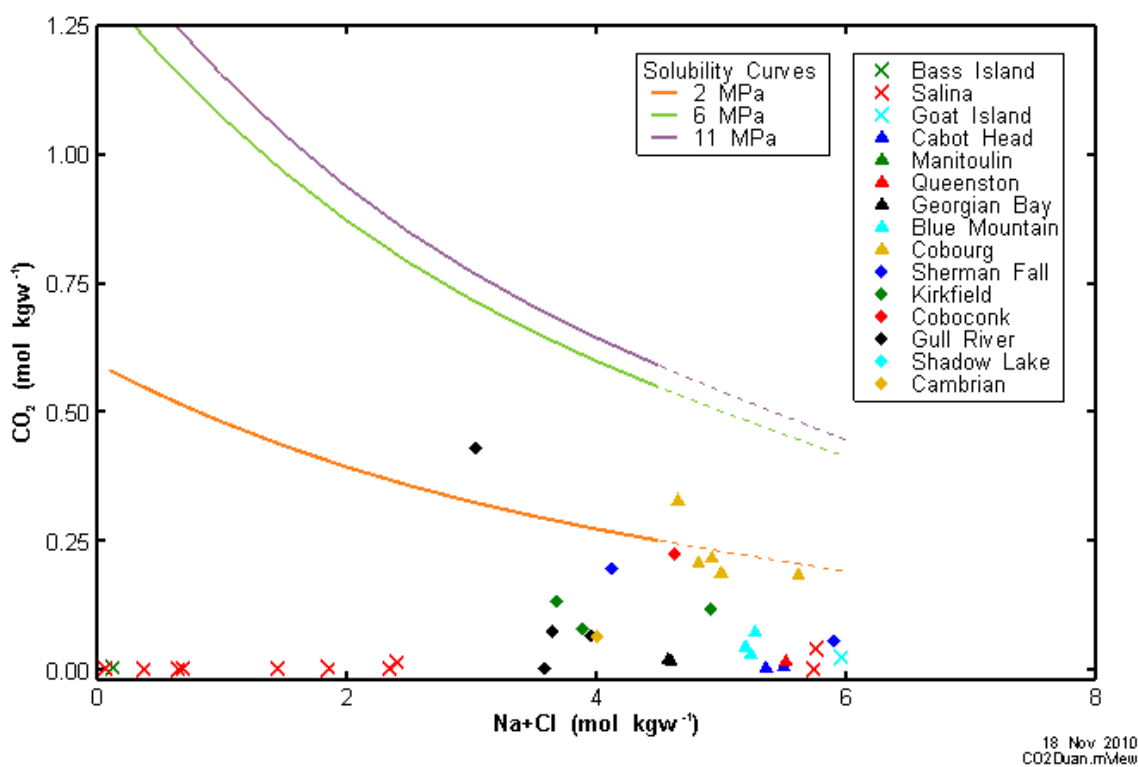


Figure 15 Cross Plot of Apparent CO₂ and Na+Cl Porewater Concentrations Compared to Calculated CO₂ Solubility in DGR-3.

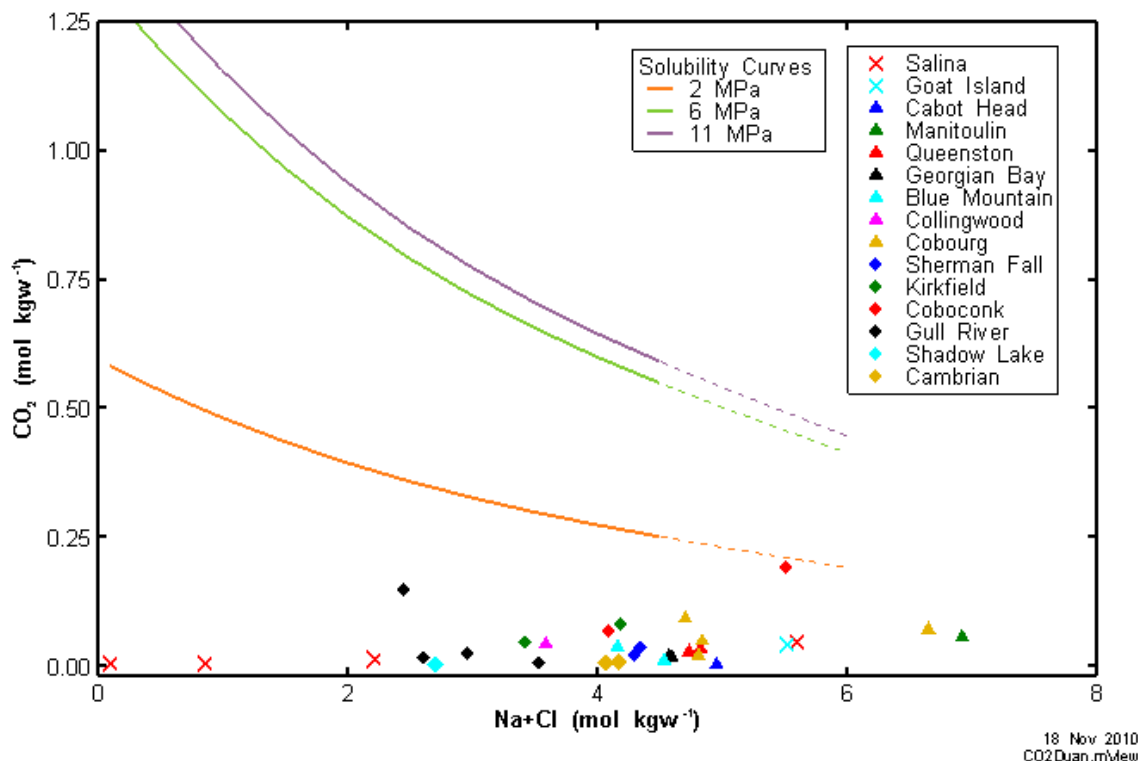


Figure 16 Cross Plot of Apparent CO₂ and Na+Cl Porewater Concentrations Compared to Calculated CO₂ Solubility in DGR-4.

Another explanation for such exceptionally low pH values is that they could potentially have been generated by in-situ degradation of hydrocarbon. A pH indicating this acidity would suggest the concurrent dissolution of calcite in the matrix in order to maintain equilibrium and would have considerably increased porosity and permeability beyond what has been determined during opportunistic groundwater sampling and laboratory testing. Therefore, a more likely scenario is that much of this CO₂ is present in a separate gas phase, as well as dissolved in brine water and any residual oil present in the pores. Corrected for such partitioning of CO₂ from the aqueous phase, calculated pH values are in the range of 5 to 6.

The dissolution of CH₄ and/or CO₂ in oil provides an enormous source for maintaining a free-gas phase in the pore system. The maximum amount of gas that can be dissolved in oil is a function of in-situ temperature, pressure and composition of the oil. The volume ratio of liberated gas to remaining oil at atmospheric pressure and 15.6°C is given by the gas-oil ratio, R_G (Mavko et al., 2009),

$$R_G = 0.02123G \left[P \exp \left(\frac{4.072}{\rho_0} - 0.00377T \right) \right]^{1.205} \quad [5]$$

where:

G = the gas gravity (i.e., the ratio of the gas density to air density at 15.6°C and atmospheric pressure),

P = the pressure in MPa, taken as the brine pressure measured at repository depth in the Cobourg Formation at a depth of approximately 680 mBGS (6 MPa),

ρ_0 = the oil density (approximated as 0.83±0.01 g/cm³ for southwestern Ontario oils (T. Carter, personal communication, April 2007), and

T = the in-situ temperature (degrees C).

Thus the gas-oil ratio expresses the tendency of the oil phase to act as an in-situ gas reservoir.

At the repository depth, approximately equivalent amounts of CH₄ and CO₂ are extracted from DGR cores (TR-07-21, TR-08-19), resulting in the gas gravity (G) of approximately 1.06, and the gas-oil ratio (R_G) of approximately 55. The in-situ pressure is in fact considerably larger than just the brine pressure measured downhole, and the total pressure (P_{TOT}) comprises brine pressure + gas pressure, which is unknown, therefore, P_{TOT} > 6 MPa. Figure 17 shows the relationship between this total pressure and the gas-oil ratio. Consequently, small oil saturations would provide a significant reservoir for CH₄ and CO₂ and result in the maintenance of a significant free-gas phase such as the gas saturations shown in Tables 5 to 9.

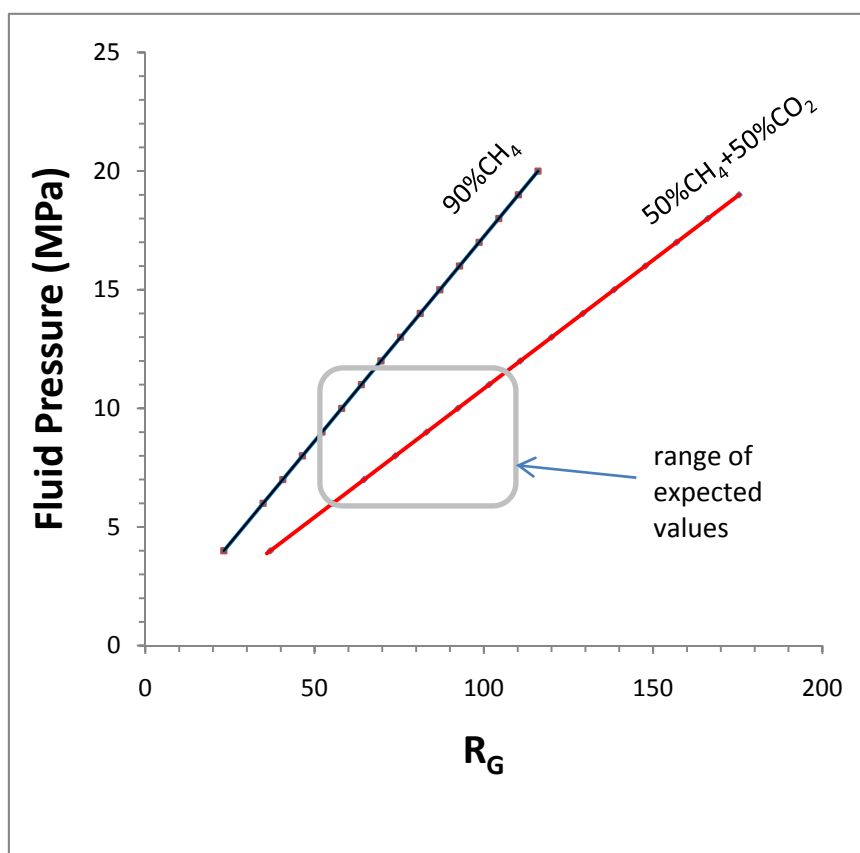


Figure 17 Gas-Oil Ratio (R_G) as a Function of In-Situ Fluid Pressure for Gases Composed of Different Amounts of Methane and Carbon Dioxide

5 Geomechanical Data

5.1 Microcrack Relaxation Porosity – Analytical Methods

Another potential source of error in estimating the gas saturation can arise when the in-situ stresses on the core are relaxed (i.e., producing dilational strain) creating new pore space measured by the petrophysical testing in the form of new microcracks that cannot completely close upon sample reloading. Such irrecoverable strains can become filled by a gas phase exsolving from the brine and any oil present in the pore. In addition to cracking due to core relaxation, irrecoverable microcrack-based strains could form due to damage during coring or sample handling and preparation. Calculations (see Section 4.2.1) indicate that the brine in the Ordovician

rocks is at saturation with methane, therefore degassing is a possible effect on the measured values. As indicated in Figure 6, the amount of core relaxation is potentially significant resulting in average porosity increases of 15 to 40%.

However, as fluid saturation testing of DGR-2, DGR-3 and DGR-4 cores is primarily based on total porosity measured under confined conditions, the amount of porosity increase that may affect gas saturations would be restricted to irrecoverable strains attributed to creation of new microcracks during sample drilling and recovery, and laboratory preparation and testing, that cannot be completely closed upon sample reloading. Such anelastic porosity increases cannot be reliably quantified from available data including geomechanical stress-strain data from uniaxial and triaxial strength testing because such data measure largely elastic strains during sample loading. The available geomechanical stress-strain data can only be used to bracket the possible range of anelastic porosity increases by assuming that a percentage of the calculated elastic relaxation porosity is due to anelastic microcrack behaviour.

Thus, to estimate the potential scale of this phenomenon, the microcrack relaxation porosity is estimated by analyzing the volumetric strain curves measured by CANMET during uniaxial and triaxial compression testing as part of the DGR-2, DGR-3 and DGR-4 geomechanical strength testing program (TR-07-03, TR-08-24, TR-09-07). This analysis, quantifies (a) the total amount of core relaxation that can be attributed to elastic microcrack behaviour, (b) estimates a likely range of anelastic porosity assuming it is a percentage of elastic relaxation porosity, and (c) assesses whether it is likely that the finite gas saturations measured during petrophysical testing of DGR cores are laboratory artefacts or are representative of in-situ conditions.

The analyses do not distinguish between microcracks formed by coring damage, sample handling and preparation, or core relaxation. It is possible that additional damage to the samples may have occurred during the coring and shaping of subsamples from the original core for testing by Core Labs (Section 3.2). However, it is unlikely that the rock samples experienced greater stresses during extraction of core plugs at Core Labs than was experienced during the original coring operation itself. Nonetheless, it is reasonable to assume that the results of the mechanical tests on full-sized core samples still provide representative, possibly conservative, estimates of the degree of overestimation of gas porosity than can be attributed to mechanical damage of the sample.

A rock sample containing microcracks will experience a change in volume when subjected to confining stress. Typically, crack deformation is nonlinear with respect to stress. In the following expression, the volumetric strain curve ($\Delta V/V$) is separated into two components representing the deformation of intact rock and that of the microcracks,

$$\frac{\Delta V}{V} = C\sigma + \phi(\sigma) \quad [6]$$

where:

C = intact rock compressibility,

σ = applied confining pressure, and

ϕ = microcrack relaxation porosity (a function of stress).

Assuming the linear portion of the volumetric strain curve represents the intact rock deformation, it is possible to project a line back to the strain axis. The intercept of this line with the volumetric strain axis represents the non-linear volumetric strain (i.e., elastic microcrack volume compression), and thus a large proportion of the porosity due to microcracks. This technique is similar to that described by Jacobsson et al. (2007).

5.2 Microcrack Relaxation Porosity Data

The results of the above analysis for 21 selected DGR-2, DGR-3 and DGR-4 core samples subject to uniaxial and triaxial compression testing is given in Appendix A. Because 9 of these 21 data sets come from uniaxial stress testing, it is possible that relaxation and microfracturing perpendicular to the horizontal (bedding) plane is greater, as the maximum principle stresses are believed to be horizontal (Lo and Morton, 1976; Lam, 2007). This might cause weakness in these samples, increasing the apparent Poisson's ratio and reducing the stress dependent volumetric strains (due to increased lateral expansion).

Ideally, analyses of this kind should be done with hydrostatically or triaxially loaded samples, rather than uniaxially loaded samples (Jacobsson et al. 2007). Triaxial stress data were collected as part of Phase 2 geomechanical laboratory testing for the Georgian Bay and Cobourg formations. These samples were loaded hydrostatically (i.e., equally stressed on all sides) up to a certain load, after which the axial load alone was increased until sample failure. The initial hydrostatic loading phase provides good quality information for assessing the volumetric amount of microcrack deformation.

Figure 18 shows this analysis for representative samples of the Georgian Bay Formation shale (DGR3-589.61) and Cobourg Formation limestone (DGR3-675.06) that were subject to triaxial compression testing. Data from triaxial compression testing are used in this example analysis because such data are likely to provide more representative estimates of volumetric strains than similar data from uniaxial compression testing, which are also given in Appendix A. It is noteworthy that the microcrack relaxation porosity determined from the geomechanical analyses (e.g., Cobourg - 0.10%) is similar to that determined from petrophysical testing of total porosity of unconfined and confined cores. This later porosity for the Cobourg is determined as unconfined total porosity [1.9% - Table 4] minus (1.9%/average ratio of unconfined/confined total porosity [1.04 – Figure 6, excluding anomalous value of 3.2]) = 0.07%. Given the uncertainty in the ratio of unconfined/confined total porosity evident in Figure 6, due to limited data for Ordovician limestones, the two estimates of microcrack relaxation porosity are considered comparable.

Comparison of the calculated relaxation porosity of the triaxially-loaded Cobourg limestone core (0.10%) and Georgian Bay shale core (0.18%) (shown in Figure 18), as well as other rocks subject to triaxial loading given in Appendix A (Figures A.10 to A.21), with those for similar rocks subject to uniaxial loading (given in Appendix A; Figures A.1 to A.9) shows they are not significantly different that the values estimated from the uniaxial compression testing. Consequently, all of the data given in Appendix A can be used to estimate the relaxation porosity for use in determining whether core relaxation is a possible explanation for observed gas saturations.

The calculated theoretical porosity change due to elastic microcrack formation and expansion during core relaxation is shown in Figure 18 as 0.18% for Georgian Bay Formation shale and 0.10% for Cobourg Formation limestone. Assuming that the anelastic porosity (created by new microcracks that cannot completely close on reloading) is 10% of the elastic porosity, the resultant anelastic porosities are 0.018% for the Georgian Bay shale and 0.01% for the Cobourg limestone. These calculated anelastic porosity increases, based on average total porosity of 7.5% and 1.9% for these formations (Figure 2, Table 3), and assuming brine incompressibility, would create equivalent gas saturations of 0.24% (i.e., 0.018/7.5) for Georgian Bay shale and 0.5% (i.e., 0.01/1.9) for Cobourg limestone. As these calculated gas saturations for the Georgian Bay shale are less than the reported average Dean Stark gas saturations of the Ordovician shales of 8.4% (Table 11 and Figure 7), it is unlikely that anelastic pore volume expansion caused by irrecoverable core relaxation can solely explain the occurrence of the reported gas saturations in the Ordovician shales.

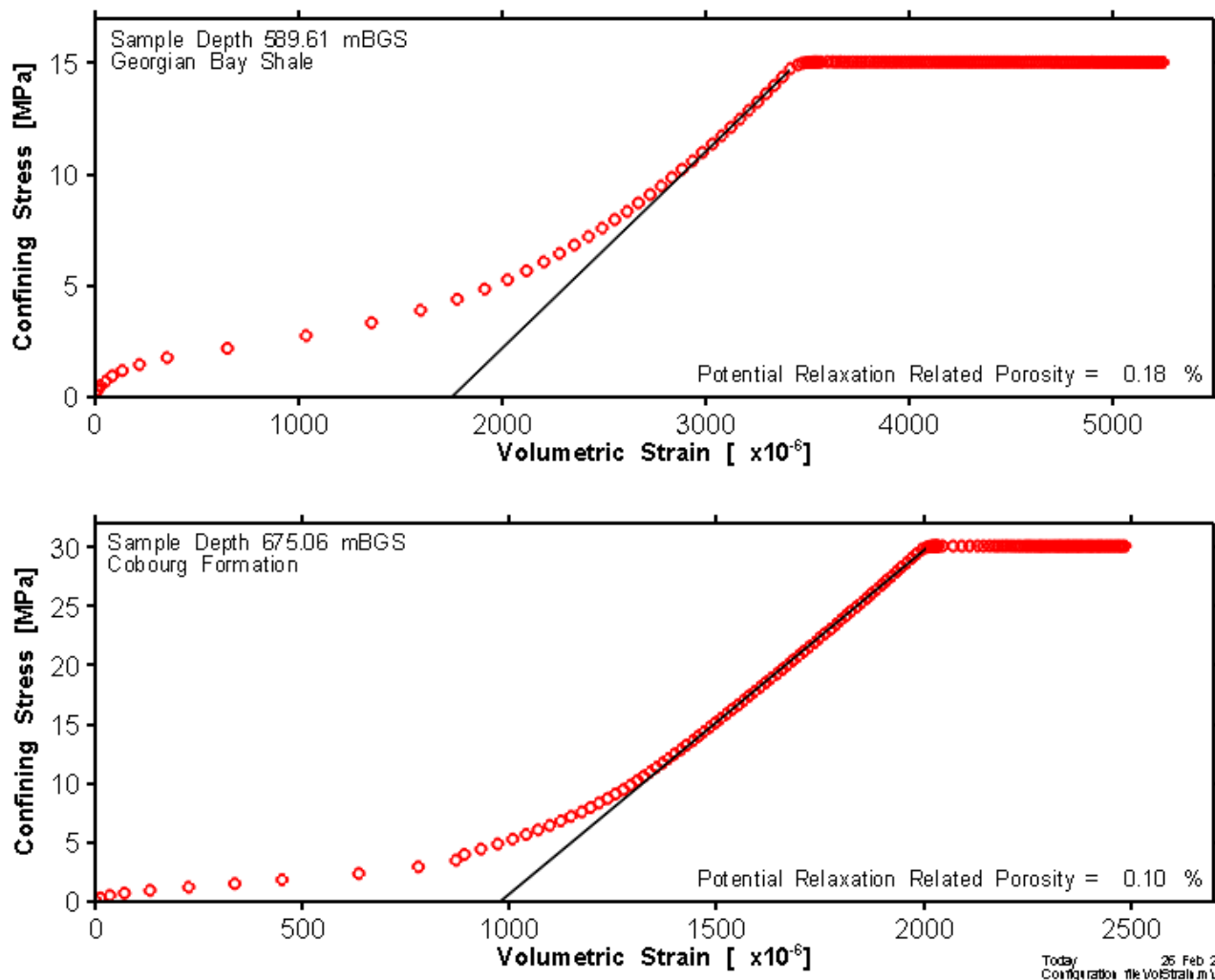


Figure 18 Determination of relaxation porosity from volumetric strain data – above Georgian Bay Formation shale (491.32 mBGS) and below Cobourg Formation limestone (675.06 mBGS) in DGR-3.

For the Cobourg and other Ordovician limestones, which have average gas saturation of 13.9% (Table 11 and Figure 7), the calculated anelastic gas saturations at 0.5% are also much smaller suggesting that the reported gas saturations are not solely artefacts of irrecoverable core relaxation. However, these conclusions for the Cobourg and other Ordovician limestones are tempered by the fact that these limestones with average porosity of 1.9% have greater fractional uncertainty in fluid saturation estimates (see Figure 11).

Figure 19 shows the measured gas-phase porosities ($S_G \times$ total porosity) and calculated microcrack relaxation porosities as listed in Appendix A. This is a conservative plot of microcrack relaxation porosity because the porosities shown are those determined assuming complete elastic response of the cores. As discussed above, the more appropriate microcrack relaxation porosity that should be plotted in Figure 19 is that due to anelastic strains due to core damage that cannot be recovered during Core Labs loading of the samples for porosity testing at hydrostatic stresses of 7 to 24 MPa, depending upon the depth of the samples. Such anelastic porosity increases will be a fraction of the relaxation porosity values shown in Figure 19.

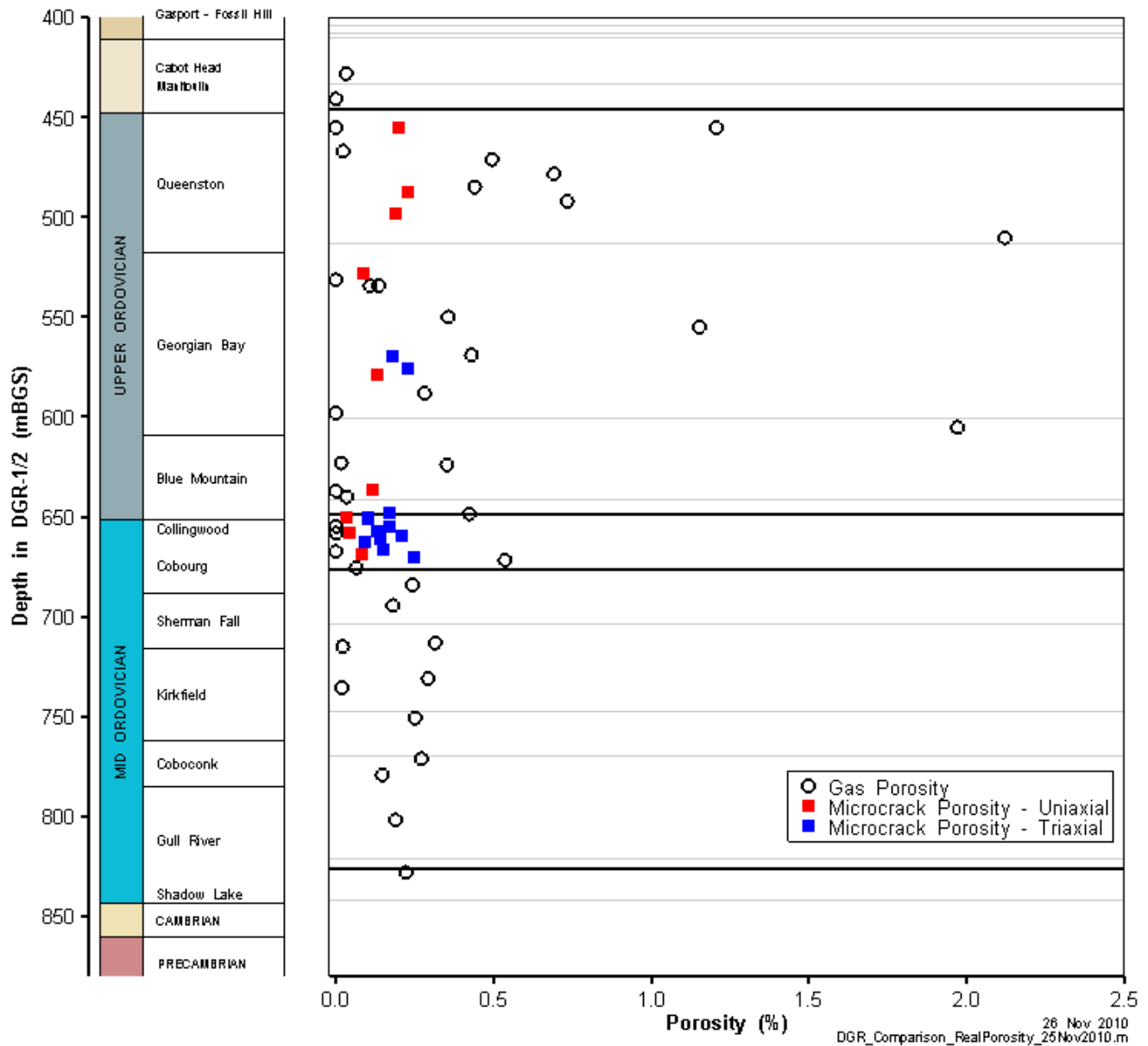


Figure 19 Profile Comparison of Gas-Phase Porosity (i.e., $S_G \times$ total porosity) and Microcrack Relaxation Porosity in DGR Cores.

Figure 19 shows there is no obvious correlation between the measured gas-phase porosity and the calculated microcrack relaxation porosity, other than the fact that more than half of the gas-phase porosities estimated from the Dean Stark extractions (Tables 5 to 9) exceed the estimated elastic microcrack relaxation porosities, particularly within the Ordovician shales. This lack of correlation and the results of the above calculations of anelastic microcrack relaxation porosity suggest that core relaxation cannot be an explanation for all reported gas saturations and hence gas-phase porosities.

Figure 19 also shows the comparison of microcrack relaxation porosities determined from uniaxial and triaxial compression testing. There does not appear to be any significant difference in the porosity values for the Ordovician shales, although there does appear to be slightly increased estimates of microcrack relaxation porosity from triaxial testing within the Collingwood and Cobourg rocks compared to that of uniaxial testing.

Given the conservative nature of Figure 19, this slight difference is not significant and does not alter the conclusions of this porosity and gas phase assessment.

6 Conclusions

Three approaches have been used to assess the presence or absence of a gas phase in the pores of the DGR rocks:

1. Petrophysical testing by Core Labs using (a) the standard Dean Stark extraction method, (b) the NMR liquid saturation method, both of which were developed for petroleum reservoir characterization, and (c) comparison of liquid vs. total porosity values;
2. Geochemical calculations of methane and carbon dioxide porewater concentrations and comparison of these concentrations to thermodynamic estimates of gas solubilities in DGR brines; and
3. Comparison of estimated core relaxation porosities from geomechanical volumetric strain analysis conducted on the DGR cores to determine if such relaxation is a possible explanation for the observed gas saturations.

An error analysis of the water saturation measurements suggest that fluid saturation estimates from Dean Stark extractions are subject to considerable error (i.e., > 50%) for the low porosity Ordovician limestones (i.e., < 3%) in the DGR sequence of rocks. Much lower error estimates are obtained for higher porosity rocks such as the Upper Ordovician shales. The average and standard deviation of gas saturations of the DGR Paleozoic rocks is $S_G = 10.9 \pm 12.0\%$, while similar values for liquid (i.e., brine) saturation are $S_W = 95.6 \pm 30.5\%$. Based on the formational average pore fluid properties presented in this report, the saturation of oil is negligible. Fluid saturation estimates from the standard Dean Stark extractions were confirmed by testing with NMR liquid saturation and $He_{(g)}$ on the same core plugs; the seven Cobourg Formation samples yielded average gas saturations of $S_G = 19.3\%$ by Dean Stark and $S_G = 19.1\%$ by $He_{(g)}$.

Assessment of total vs. liquid porosity measurements supports the presence of a gas phase, whereby approximately 70% of the lower porosity Ordovician limestones exhibited a liquid porosity less than total porosity (40-50% of the Ordovician shales and Devonian and Silurian formations). The total and liquid porosity values are difficult to compare between laboratories, or even adjacent samples, due to the variability in porosity measurement methodology and sample size; therefore, this dataset provides supporting evidence which is not conclusive on its own.

Comparison of the lab measured methane concentrations in DGR cores to thermodynamic estimates of methane solubility considering porewater chemistry, temperature and formation pressure shows that many of the methane concentrations exceed solubility limits, particularly in the Collingwood/Cobourg and Blue Mountain formations and to a lesser degree in the Salina A1 Unit, Manitoulin, Georgian Bay, Kirkfield and Gull River formations. These exceedences of solubility limits suggest that separate methane gas phase may be present. Similar calculations for carbon dioxide indicate that a separate carbon dioxide gas phase is not likely present.

The volumetric strain analysis shows that the volume attributable to microcracks, which likely represents the majority of pore volume expansion due to core relaxation, is far below the measured pore volume occupied by gas for many of the core samples, especially those from the Ordovician shales. Further, the total porosity measurements were performed under confining stress of at least 7 MPa. For all samples, the great majority of microcracks were closed above 7 MPa. This suggests that total porosities measured during the petrophysical testing should be reasonably representative of in-situ porosity values. Thus, microcracking due to core relaxation cannot be used as an explanation for the apparent gas saturations in the Ordovician and Silurian sequences at the Bruce nuclear site.

Consequently these results indicate that the fluid saturation values presented in this report (Tables 5 to 9) are suitable for preliminary use in the DGR program.

7 References

Curtis, J.B. 2002. Fractured shale-gas systems. AAPG Bulletin, Vol. 86, No.11, pp.1921-1938.

Duan, Z. and S. Mao. 2006. A thermodynamic model for calculating methane solubility, density and gas phase composition of methane-bearing aqueous fluids from 273 to 523 °K and from 1 to 2000 bar, *Geochimica et Cosmochimica Acta*, Vol. 70, pp. 3369–3386.

Duan, Z. and R. Sun. 2003. An improved model calculating CO₂ solubility in pure water and aqueous NaCl solutions from 273 to 533 °K and from 0 to 2000 bar, *Chemical Geology*, Vol. 193, No. 3-4, pp. 257-271

Geofirma Engineering Ltd., 2011a. Technical Report: Laboratory Petrophysical Testing of DGR-5 and DGR-6 Core, TR-09-08, Revision 0, April 7, Ottawa

Geofirma Engineering Ltd., 2011b. Technical Report: Porewater Analyses in DGR-5 and DGR-6 Core, TR-09-04, Revision 0, April 15, Ottawa.

Geofirma Engineering Ltd., 2011c. Technical Report: Laboratory Geomechanical Strength Testing of DGR-2 to DGR-6 Core, TR-09-07, Revision 0, April 7, Ottawa.

Geofirma Engineering Ltd., 2011d. Technical Report: Pressure and Head Monitoring in MP55 Casings Installed in DGR-1 to DGR-4, TR-08-31, Revision 0, April 14, Ottawa.

Hobbs, M.Y., A. de Haller,, M. Koroleva, M. Mazurek, J. Spangenberg, U. Mader, and D. Meier, 2011. Borehole DGR-3 and DGR-4 Porewater Investigations, Intera Engineering Ltd., Technical Report TR-08-40, March 31, Institute of Geological Sciences, University of Bern, Switzerland.

Intera Engineering Ltd., 2010a. Technical Report: Laboratory Petrophysical Testing of DGR-2 Core, TR-07-18, Revision 2, May 20, Ottawa.

Intera Engineering Ltd., 2010b. Technical Report: Laboratory Petrophysical Testing of DGR-3 and DGR-4 Core. TR-08-28, Revision 0, February 23, Ottawa.

Intera Engineering Ltd., 2010c. Technical Report: Pore Water and Gas Analyses in DGR-1 and DGR-2 Core, TR-07-21, Revision 1, May 20.

Intera Engineering Ltd., 2010d. Technical Report: Laboratory Diffusion Testing of DGR-2 Core, TR-07-17, Revision 3, May 19, Ottawa.

Intera Engineering Ltd., 2010e. Technical Report: Porewater and Gas Analyses of DGR-3 and DGR-4 Core, TR-08-19, Revision 0, June 3, Ottawa.

Intera Engineering Ltd., 2010f. Technical Report: Laboratory Diffusion Testing of DGR-3 and DGR-4 Core, TR-08-27, Revision 0, May 7, Ottawa.

Intera Engineering Ltd., 2010g. Technical Report: Opportunistic Groundwater Sampling in DGR-1 & DGR-2, TR-07-11, Revision 2, May 19, Ottawa.

- Intera Engineering Ltd., 2010h. Technical Report: Initial Groundwater Monitoring, US-3, US-7, and US-8, TR-08-08, Revision 1, June 29, Ottawa.
- Intera Engineering Ltd., 2010i. Technical Report: Opportunistic Groundwater Sampling in DGR-3 and DGR-4, TR-08-18, Revision 1, June 18, Ottawa.
- Intera Engineering Ltd., 2010j. Technical Report: Laboratory Geomechanical Strength Testing of DGR-3 and DGR-4 Core, TR-08-24, Revision 1, June 18, Ottawa.
- Intera Engineering Ltd., 2009a. Project Quality Plan, DGR Site Characterization, Revision 4, August 14, Ottawa.
- Intera Engineering Ltd., 2009b. Technical Report: Laboratory Geomechanical Strength Testing of DGR-1 and DGR-2 Core, TR-07-03, Revision 3, February 3, Ottawa.
- Intera Engineering Ltd., 2009c. Test Plan for Laboratory Petrophysical Testing of DGR-5 and DGR-6 Core, TP-09-08, Revision 1, August 17, Ottawa.
- Intera Engineering Ltd., 2008a. Phase 2 Geoscientific Site Characterization Plan, OPG's Deep Geologic Repository for Low and Intermediate Level Waste, Report INTERA 06-219.50-Phase 2 GSCP-R0. OPG 00216-PLAN-03902-00002-R00, April.
- Intera Engineering Ltd., 2008b. Test Plan for Laboratory Petrophysical Testing of DGR-3 and DGR-4 Core, TP-08-11, Revision 0, June 10, Ottawa.
- Intera Engineering Ltd., 2008c. Test Plan for DGR-3 & DGR-4 Core Sampling and Distribution for Laboratory Testing, TP-08-04, Revision 6, September 28, Ottawa.
- Intera Engineering Ltd., 2008d. Test Plan for Laboratory Testing of DGR-3 and DGR-4 Cores for Pore-Water Extraction and Analysis, TP-08-10, Revision 1, December 3, Ottawa.
- Intera Engineering Ltd., 2007a. Test Plan for Laboratory Petrophysical Testing of DGR-3 & DGR-4 Core, TP-07-03, Revision 1, May 28, Ottawa.
- Intera Engineering Ltd., 2007b. Test Plan for DGR-1 and DGR-2 Core Sampling and Distribution, TP-06-10, Revision 4, May 14, Ottawa
- Intera Engineering Ltd., 2006. Geoscientific Site Characterization Plan, OPG's Deep Geologic Repository for Low and Intermediate Level Waste, Report INTERA 05-220-1, OPG 00216-REP-03902-00002-R00, April.
- Jacobsson, L., M. Flansbjer, R. Christiansson and T. Janson, 2007. Measurement of micro crack volume in low porosity crystalline rock, Proceedings of the 11th International Congress on Rock Mechanics, Lisbon, Portugal, 2007.
- Koroleva, M., A. de Haller, U. Mader, H.N. Mader and M. Mazurek. 2009. Borehole DGR-2: Pore-water investigations. Intera Engineering Ltd., Technical Report TR-08-06, August 4, Institute of Geological Sciences, University of Bern, Switzerland.
- Lam, T., 2007. Deep Geologic Repository for Low and Intermediate Level Waste Regional Geomechanical Property and In-situ Stress Databases, File number: 00216-03921-T10, May 2007, Ontario Power Generation.
- Lo, K.Y. and J.D. Morton. 1976. Tunnels in bedded rock with high horizontal stresses. Canadian Geotechnical Journal, Vol. 13, pp. 216-230.

Lucia, F.J. 1999. Carbonate Reservoir Characterization. Springer, New York.

Mavko, R., T. Mukerji and J. Dvorkin, 2009. The Rock Physics Handbook: Tools for Seismic Analysis of Porous Media. Cambridge University Press, New York.

Neuzil, C.E. 1993. Low fluid pressure within the Pierre Shale: A transient response to erosion, Water Resources Research, Vol. 29, No.7, pp.2007-2020.

Neuzil, C.E. and D.W. Pollock. 1982. Erosional unloading and fluid pressures in hydraulically 'tight' rocks, American Journal of Science, Vol. 91, pp.179-193.

Pearson, F.J., 1999. What's the porosity of a mudrock? Geological Society of London, Special Publications; Volume 158, pp. 9-21.

Stoessell, R.K. and P.A. Byrne. 1982. Salting-out of methane in single-salt solutions at 25°C and below 800 psia, Geochimica et Cosmochimica Acta, Vol.46, pp. 1327–1332.

Woodhouse, R. 1998. Determinations of Uncertainty in S_w . Appendix to Accurate reservoir water saturations from oil-mud cores: Questions and answers from Prudhoe Bay and beyond. The Log Analyst, May-June issue, pp. 44-47.

APPENDIX A
Volumetric Strain Curves – DGR-2, DGR-3 and DGR-4 Cores
Figures A.1 to A.21

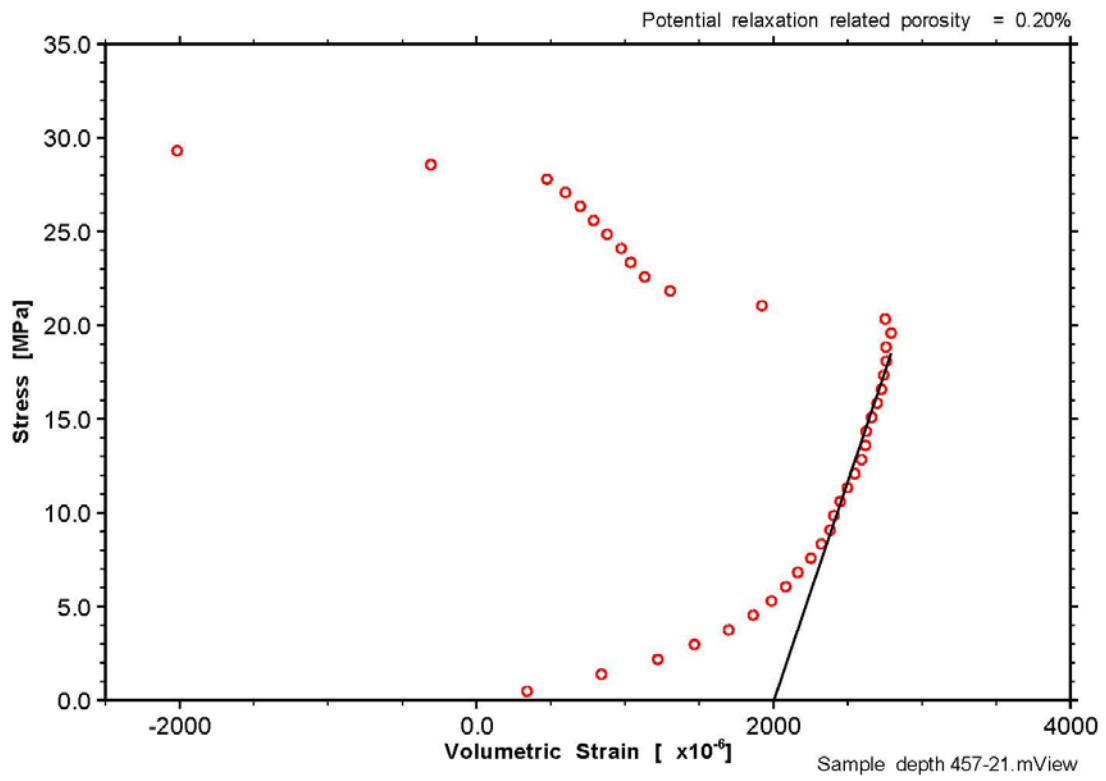


Figure A.1 Uniaxial volumetric strain curve from sample DGR2-457.21, Queenston Formation.

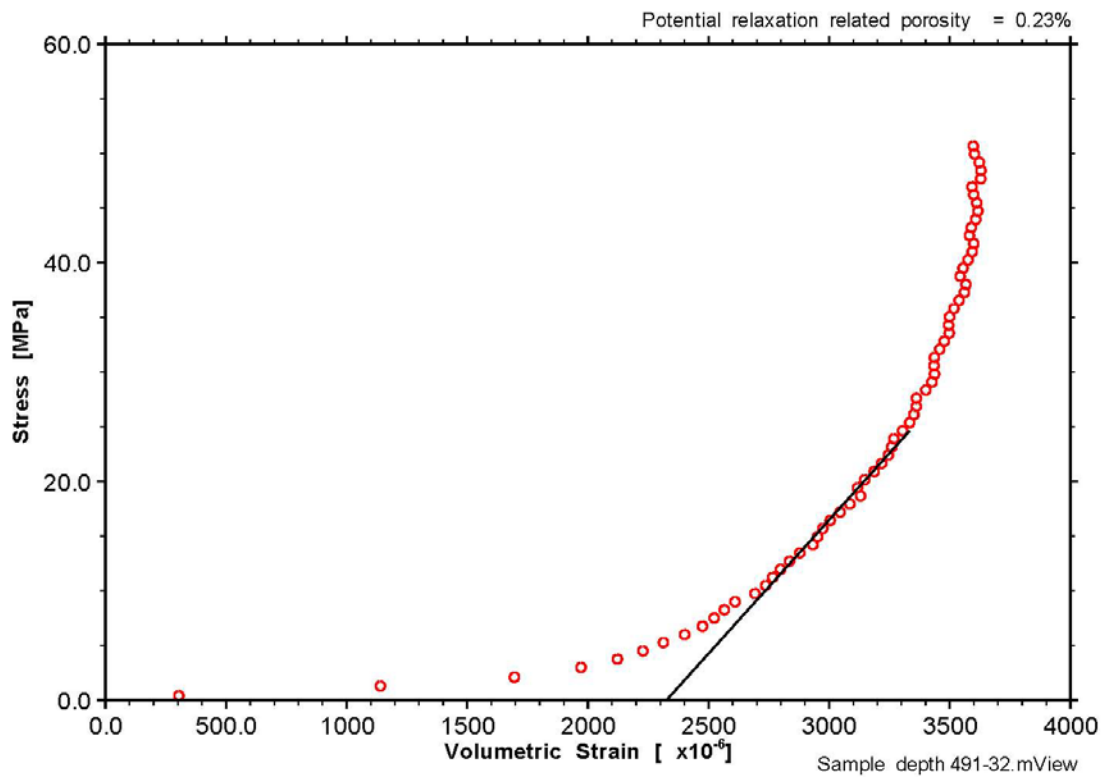


Figure A.2 Uniaxial volumetric strain curve from DGR2-491.32, Queenston Formation

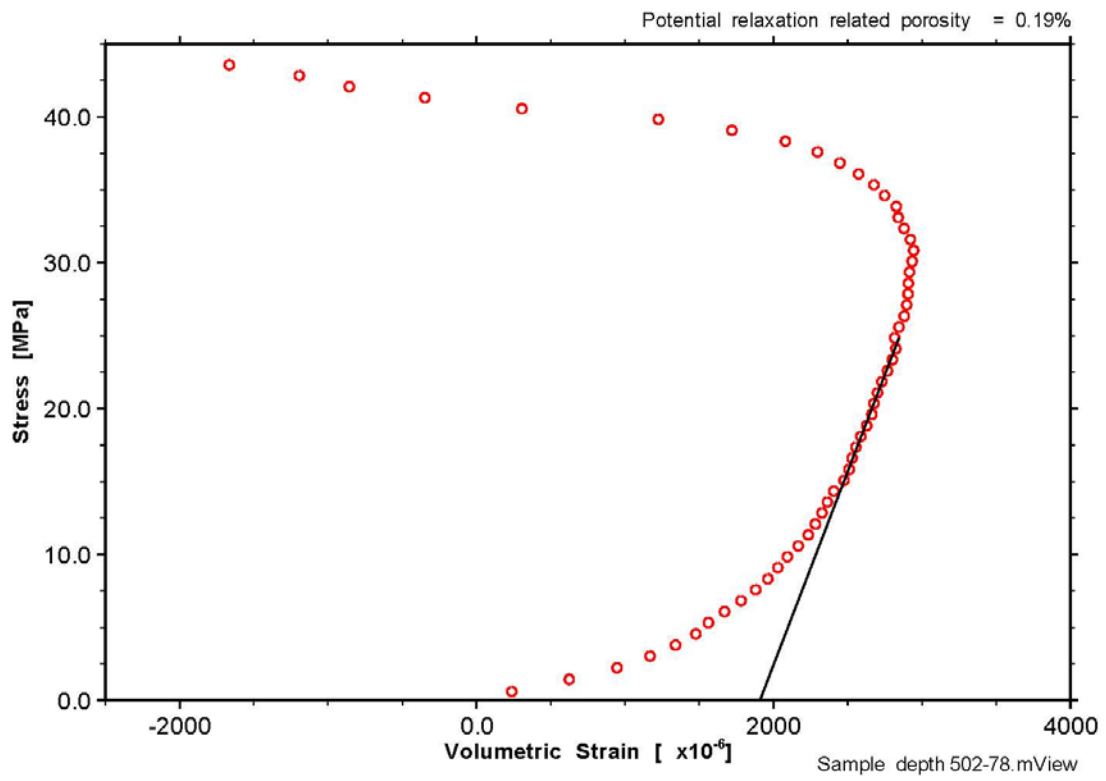


Figure A.3 Uniaxial volumetric strain curve from DGR2-502.78, Queenston Formation

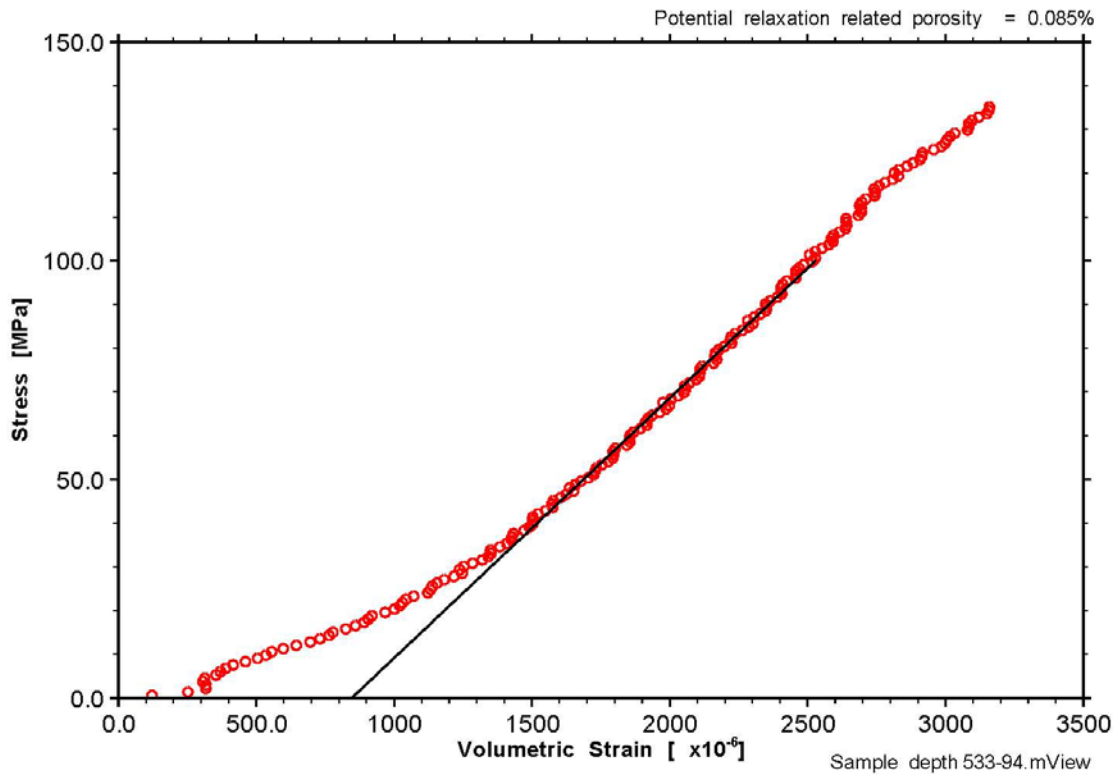


Figure A.4 Uniaxial volumetric strain curve from DGR2-533.94, Georgian Bay Formation

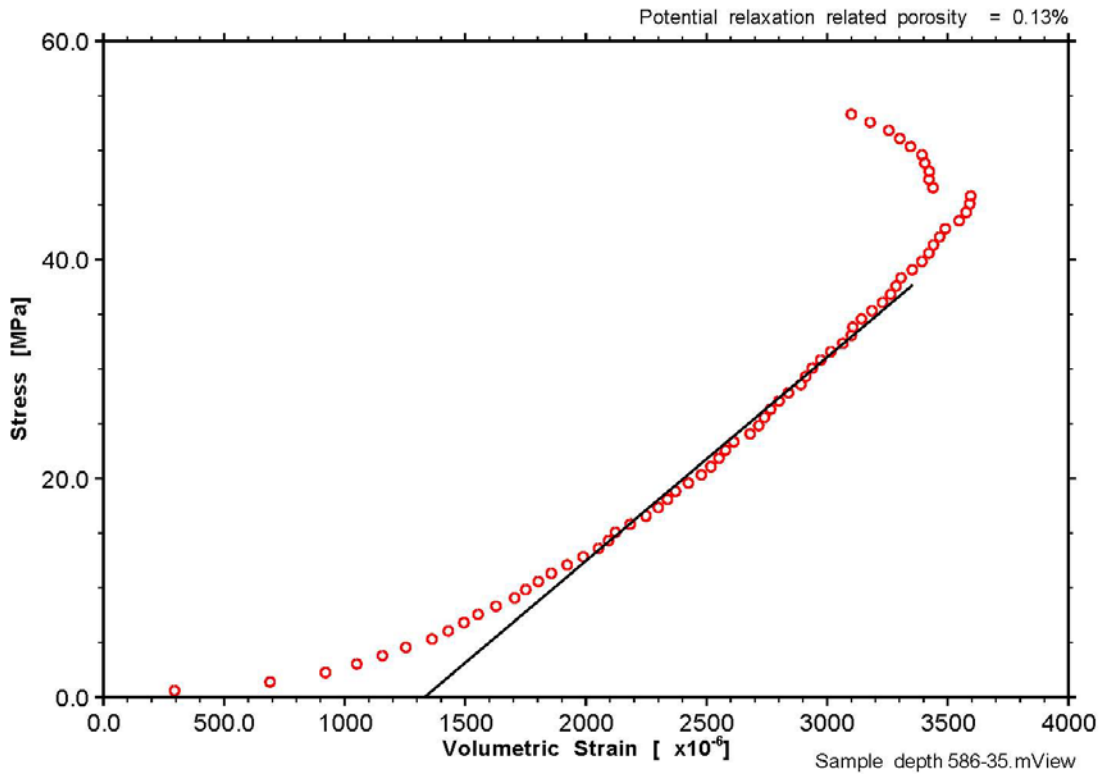


Figure A.5 Uniaxial volumetric strain curve from DGR2-586.35, Georgian Bay Formation

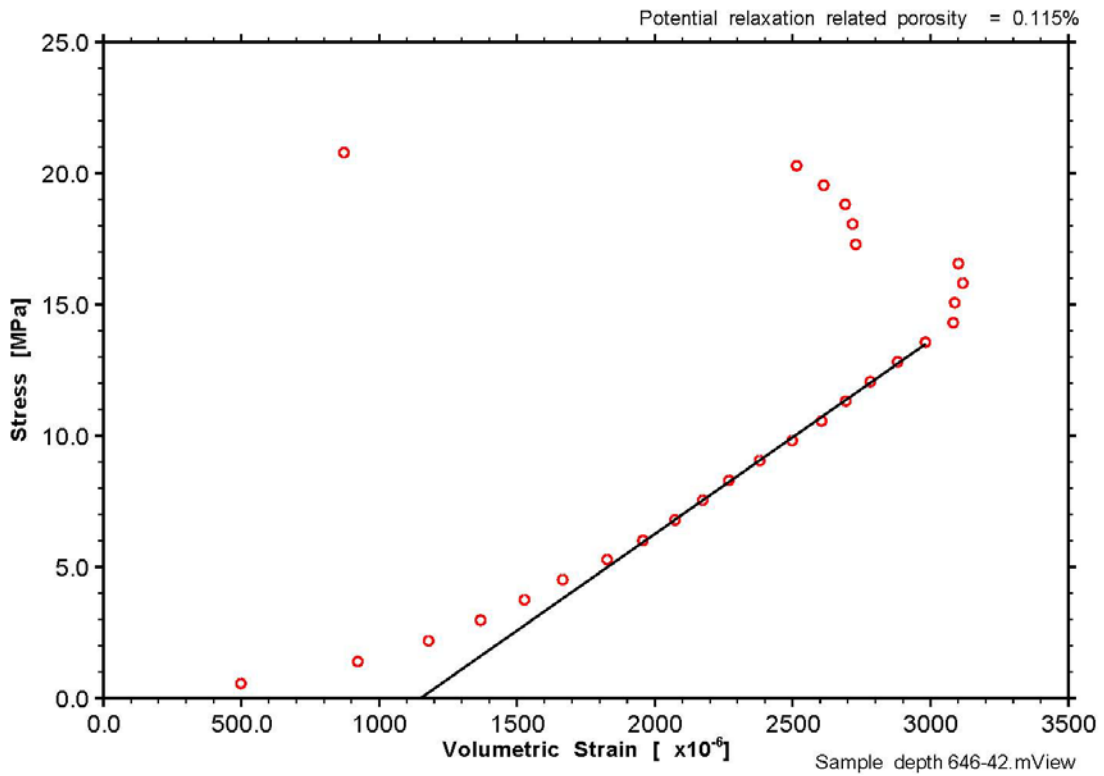


Figure A.6 Uniaxial volumetric strain curve from sample DGR2-646.42, Blue Mountain Formation

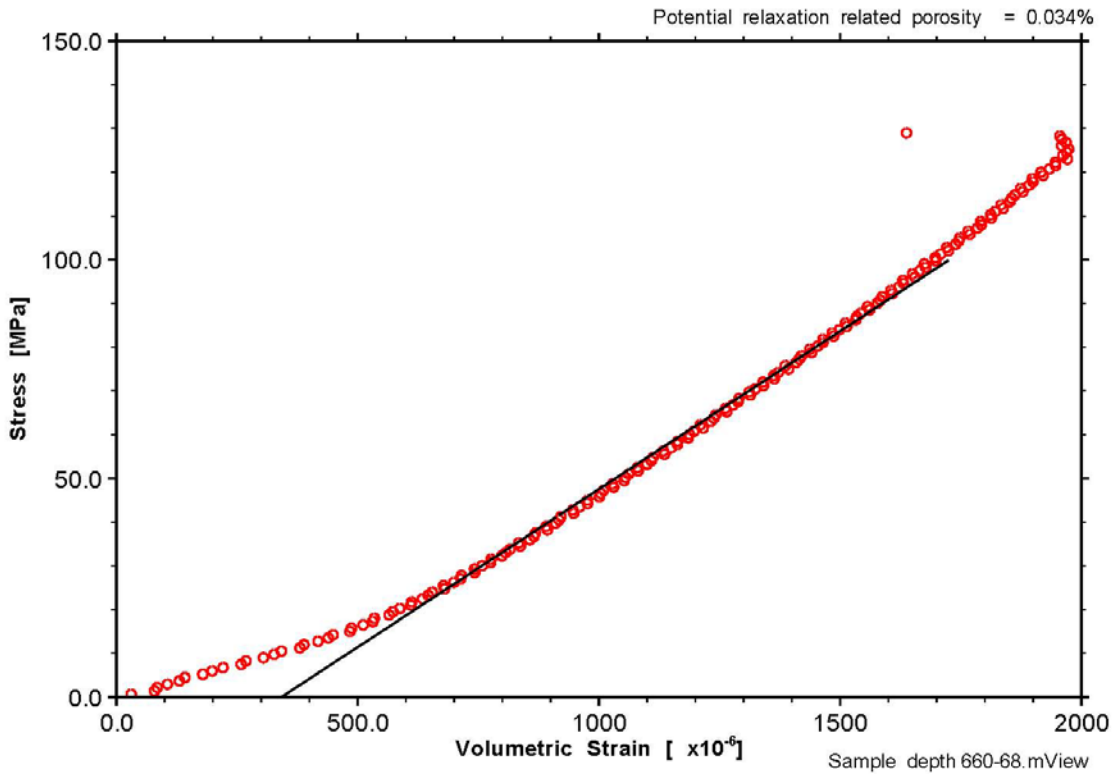


Figure A.7 Uniaxial volumetric strain curve from DGR2-660.68, Cobourg Formation

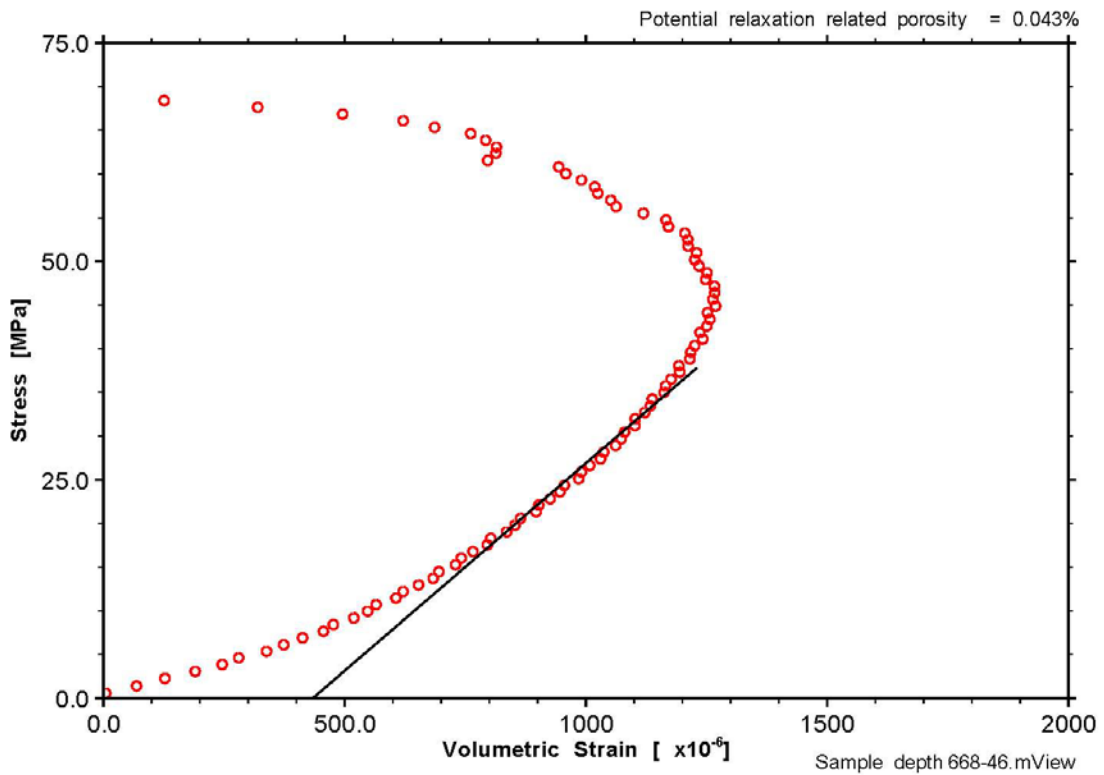


Figure A.8 Uniaxial volumetric strain curve from DGR2-668.46, Cobourg Formation

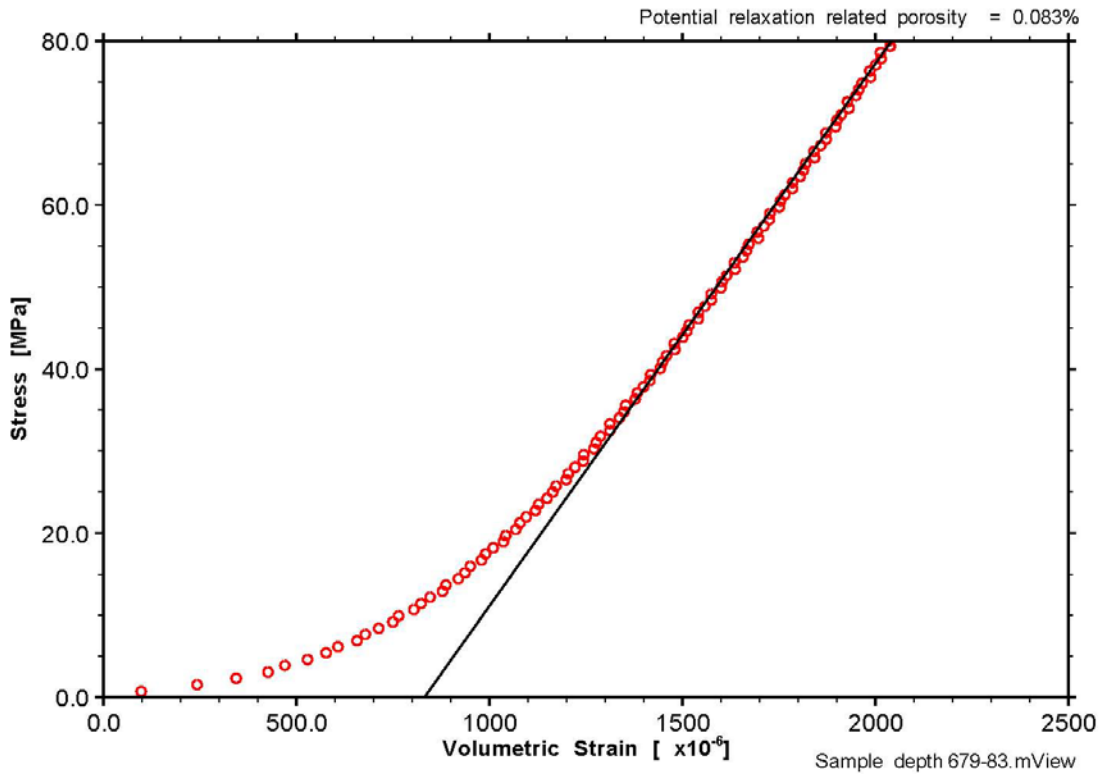


Figure A.9 Uniaxial volumetric strain curve from DGR2-679.83, Cobourg Formation

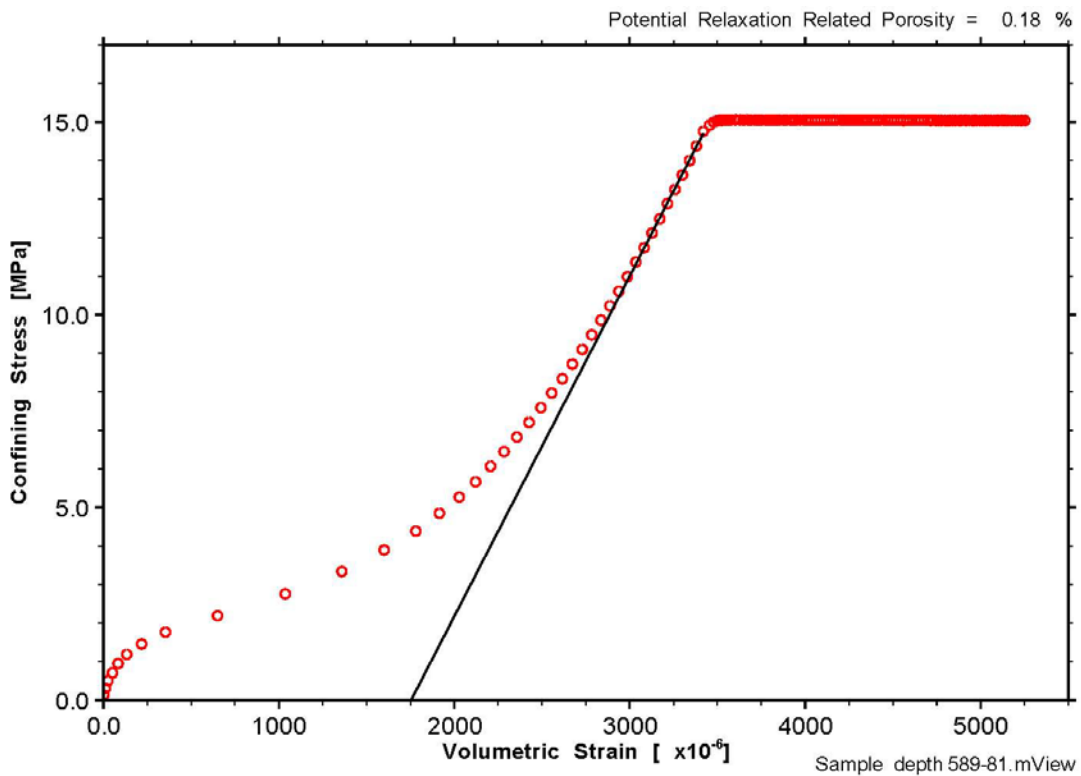


Figure A.10 Triaxial volumetric strain curve from DGR3-589.61, Georgian Bay Formation

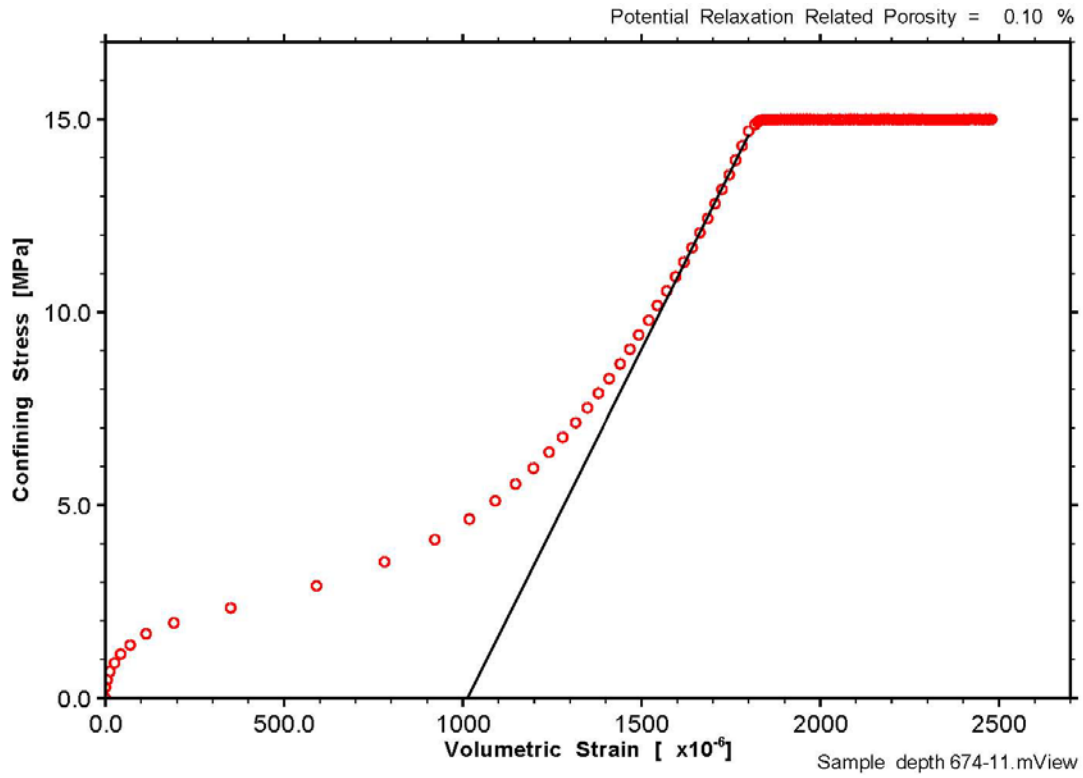


Figure A.11 Triaxial volumetric strain curve from DGR3-674.11, Cobourg Formation

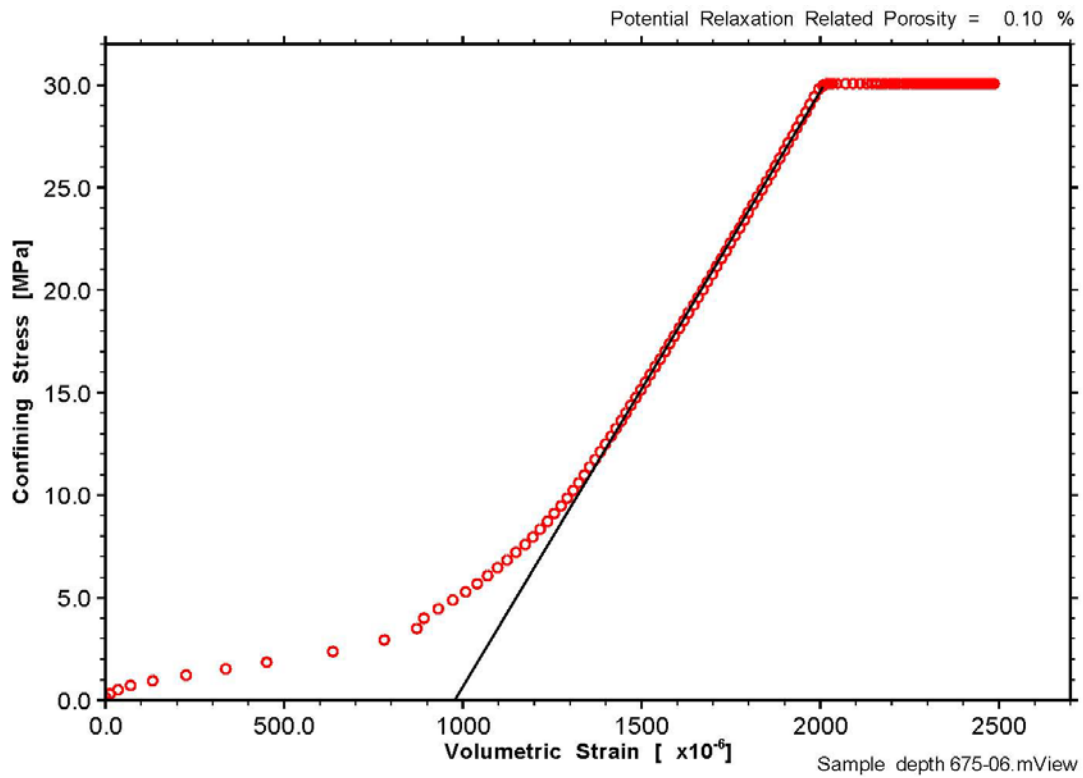


Figure A.12 Triaxial volumetric strain curve from DGR3-675.06, Cobourg Formation

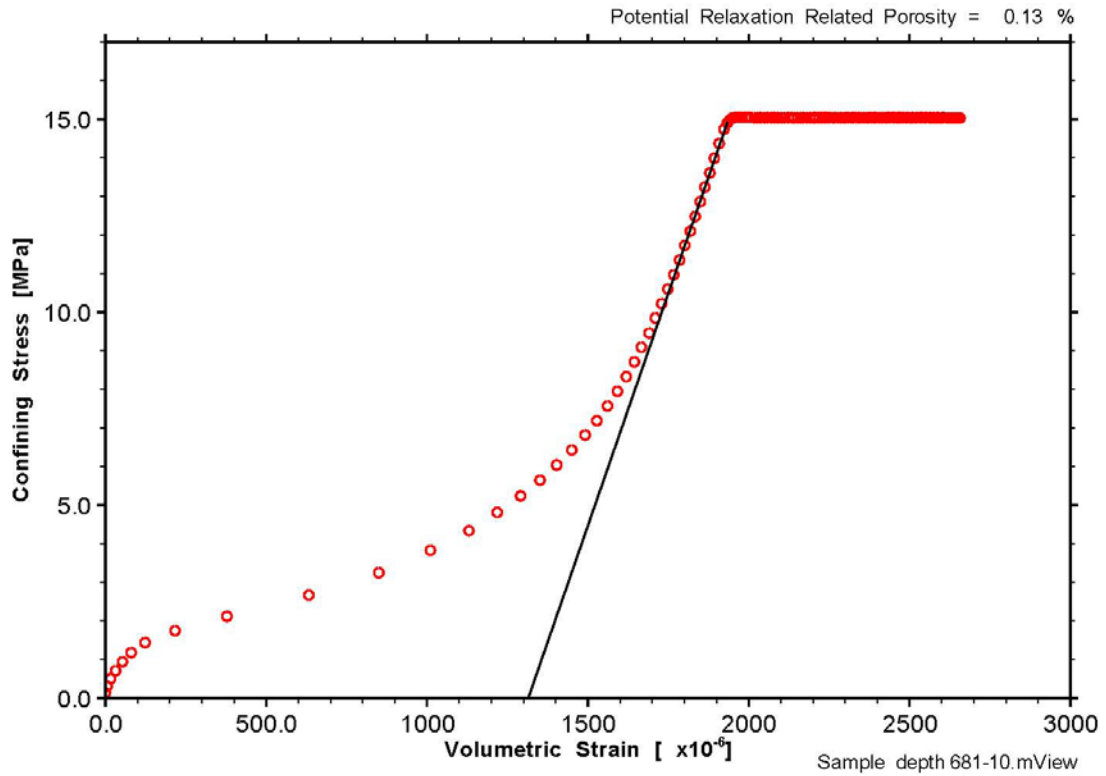


Figure A.13 Triaxial volumetric strain curve from DGR3-681.10, Cobourg Formation

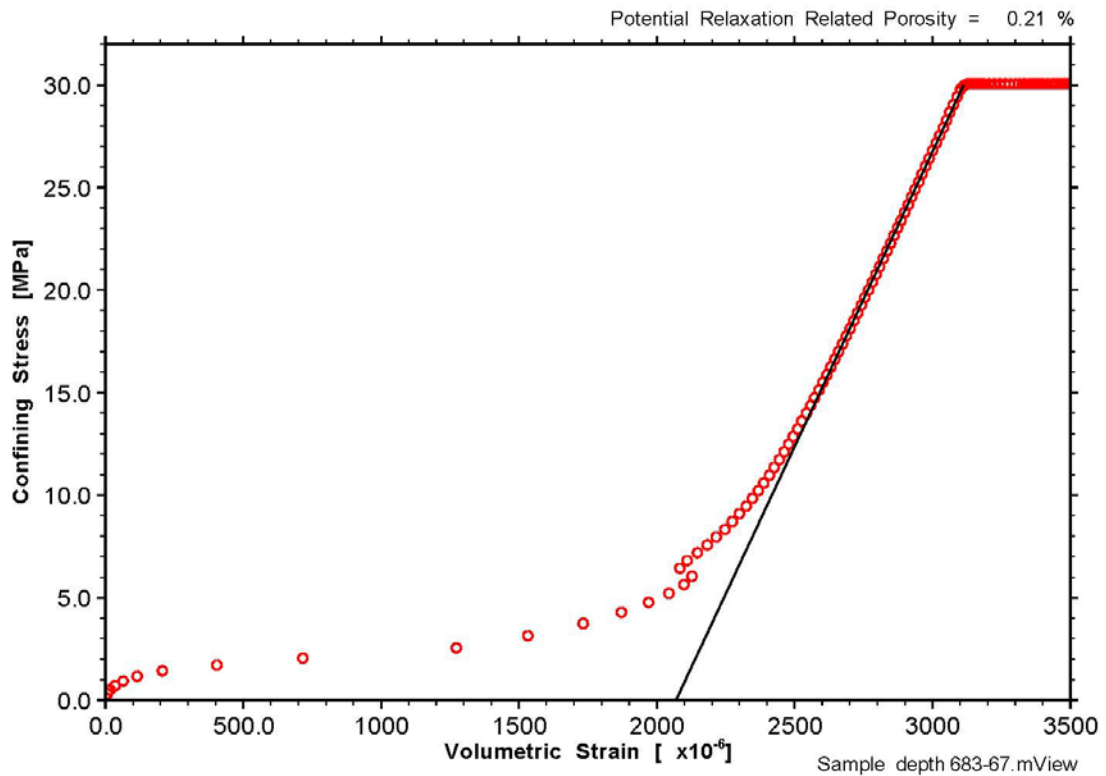


Figure A.14 Triaxial volumetric strain curve from DGR3-683.67, Cobourg Formation

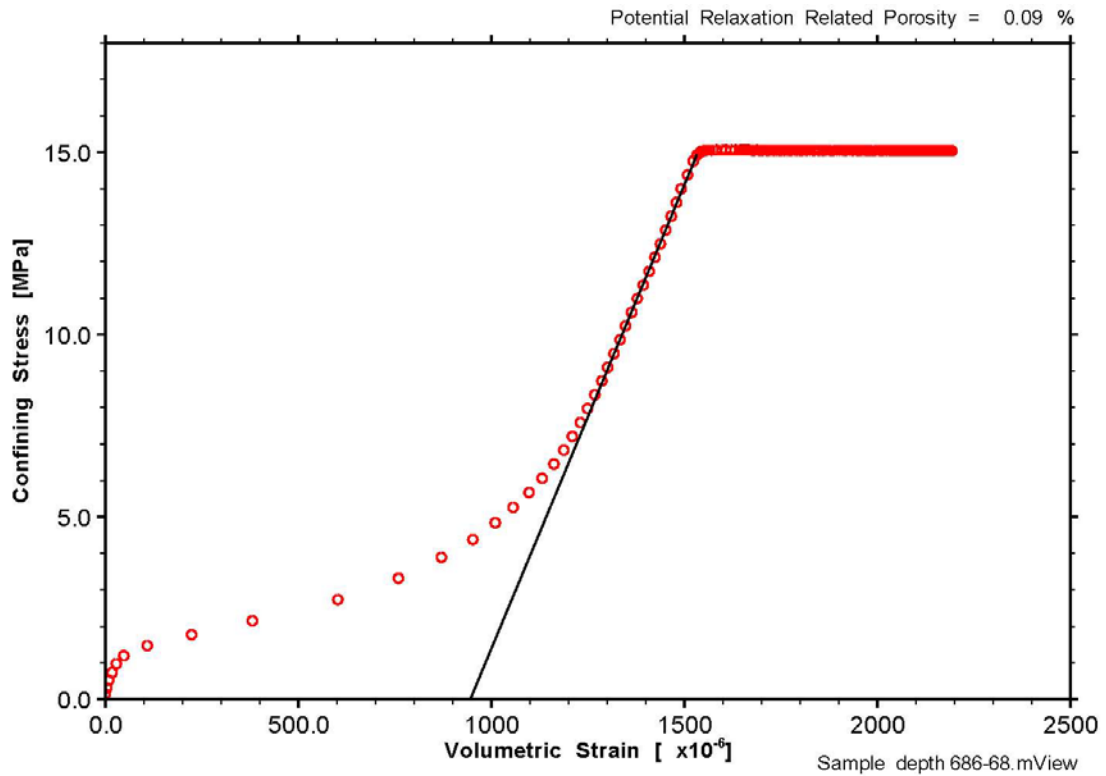


Figure A.15 Triaxial volumetric strain curve from DGR3-686.68, Cobourg Formation

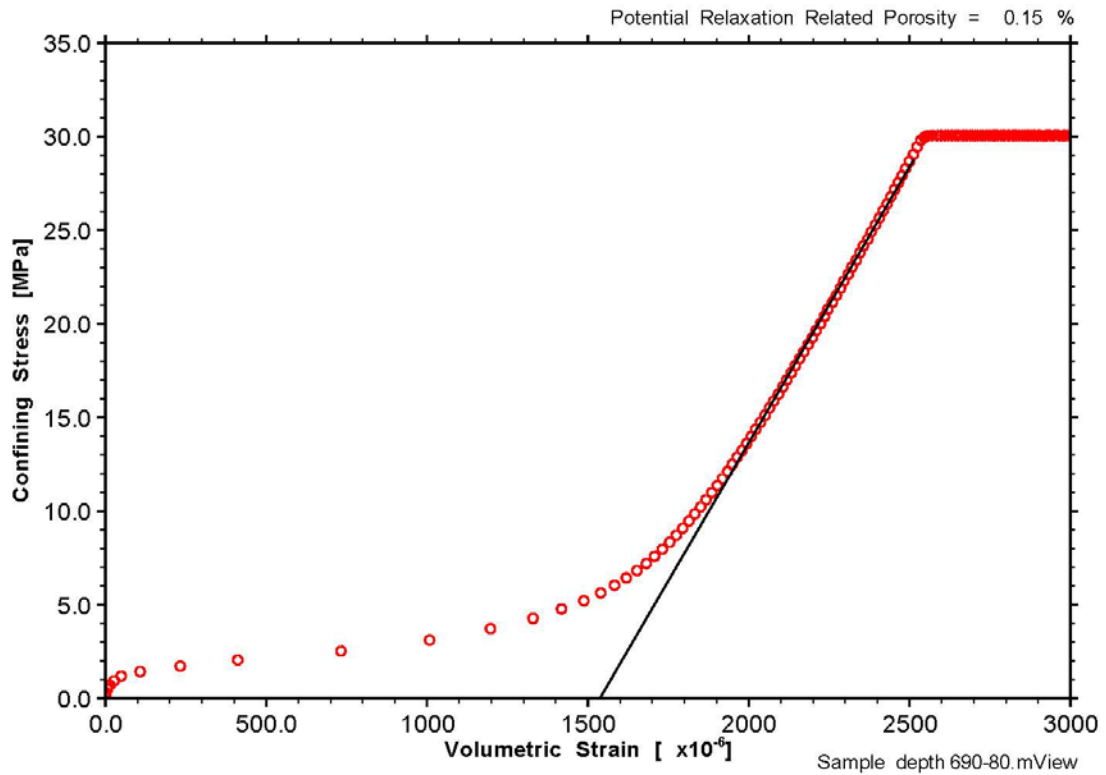


Figure A.16 Triaxial volumetric strain curve from DGR3-690.80, Sherman Fall Formation

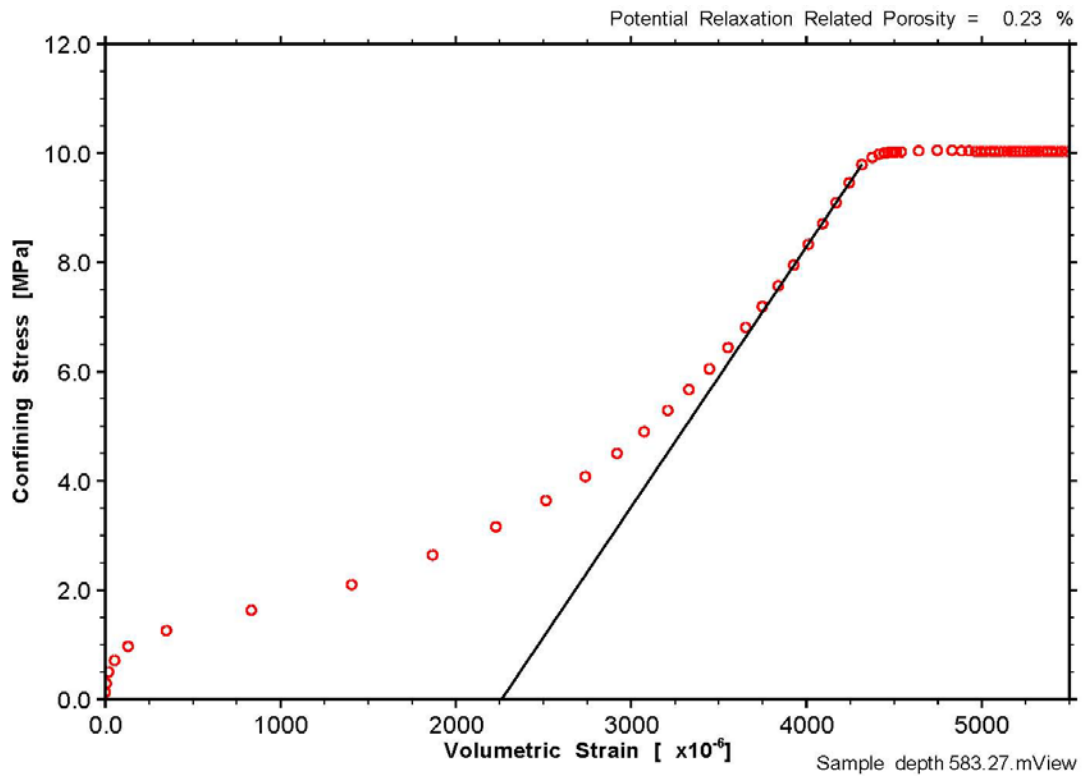


Figure A.17 Triaxial volumetric strain curve from DGR4-583.27, Georgian Bay Formation

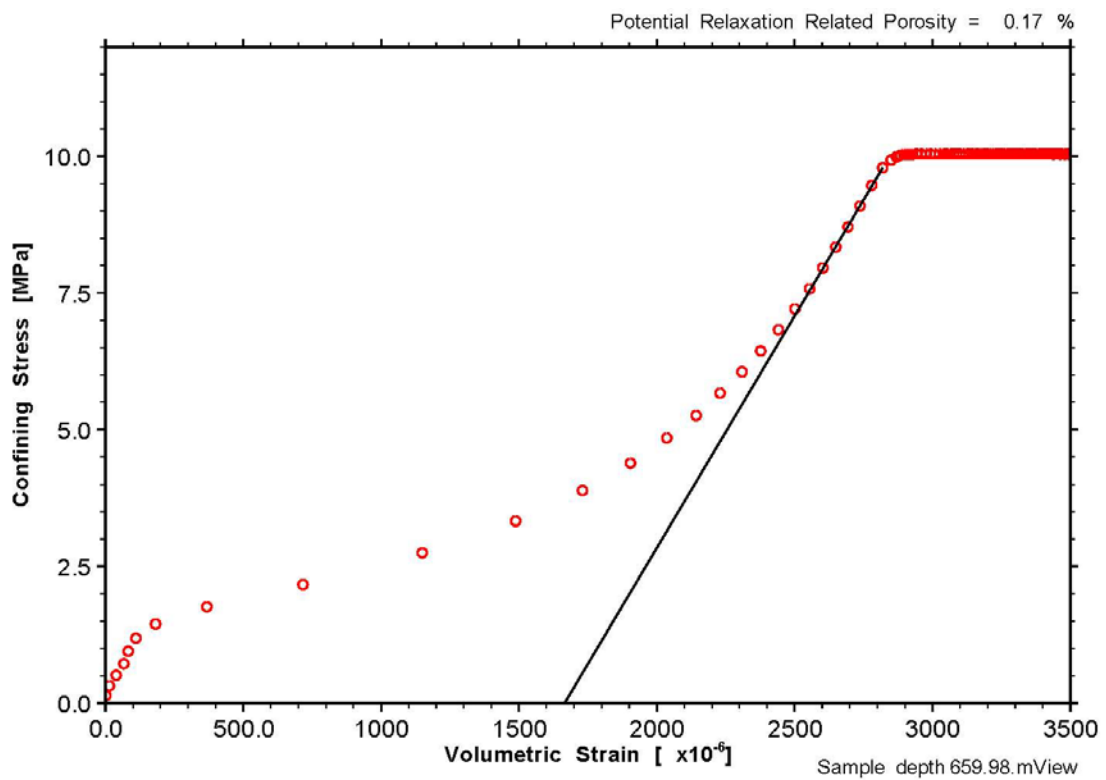


Figure A.18 Triaxial volumetric strain curve from DGR4-659.98, Collingwood Member

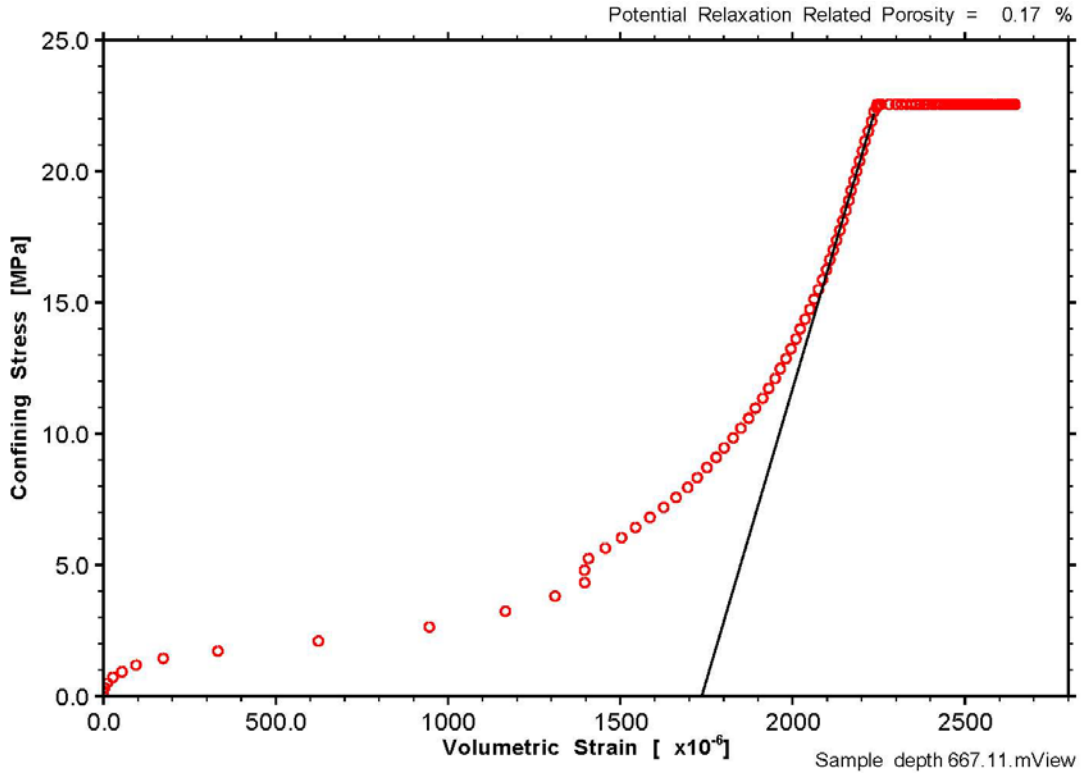


Figure A.19 Triaxial volumetric strain curve from DGR4-667.11, Cobourg Formation

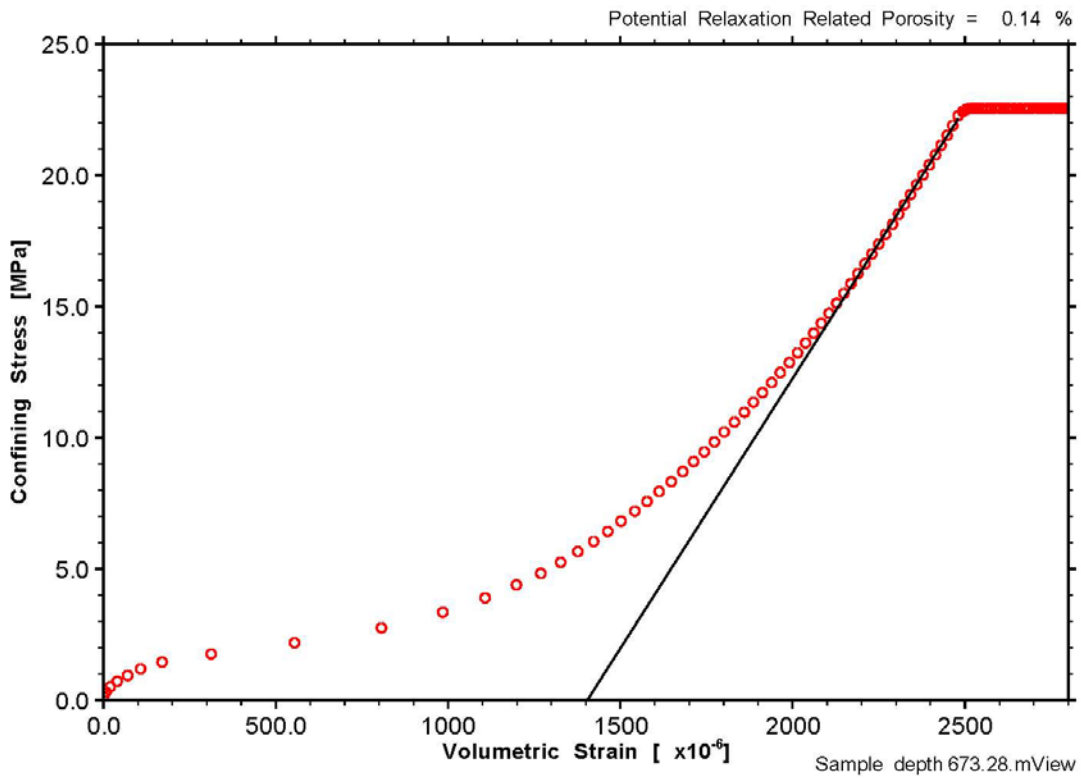


Figure A.20 Triaxial volumetric strain curve from DGR4-673.28, Cobourg Formation

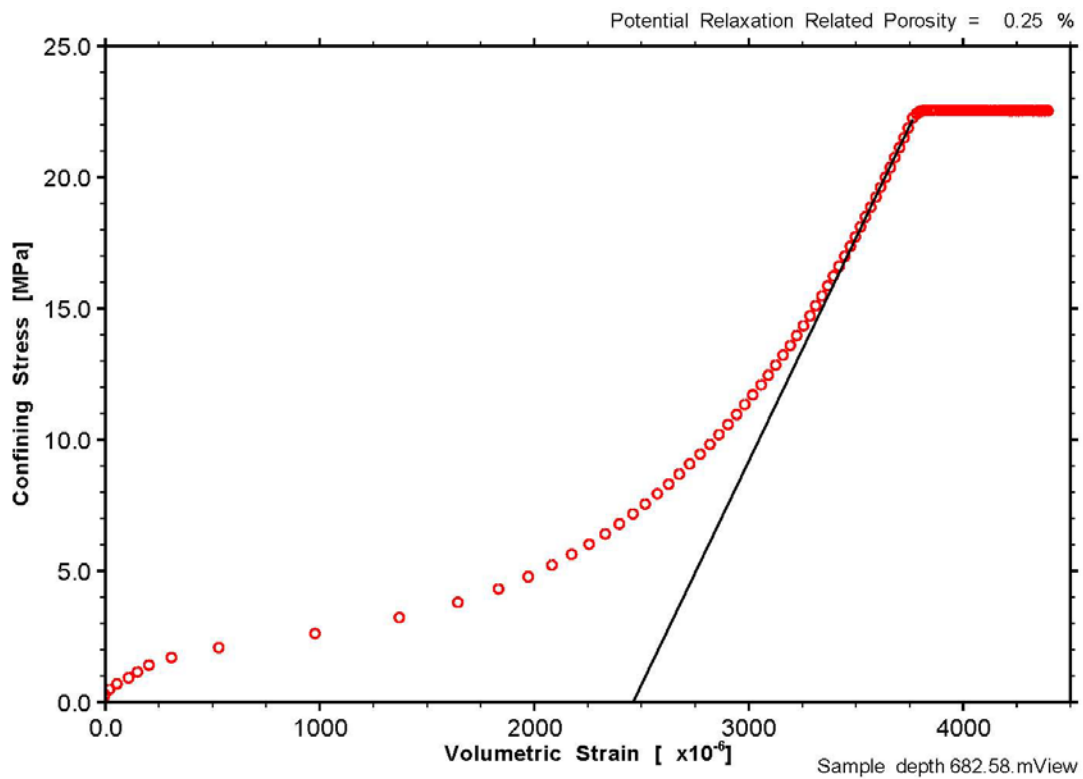


Figure A.21 Triaxial volumetric strain curve from DGR4-682.58, Cobourg Formation